Interaction-Driven Metal-Insulator Transition with Charge Fractionalization

Yichen Xu,[1] Xiao-Chuan Wu,[1] Mengxing Ye,[2] Zhu-Xi Luo,[2] Chao-Ming Jian,[3] and Cenke Xu[1]
[1]*Department of Physics, University of California, Santa Barbara, California 93106, USA*
[2]*Kavli Institute for Theoretical Physics, University of California, Santa Barbara, California 93106, USA*
[3]*Department of Physics, Cornell University, Ithaca, New York 14853, USA*

(Received 18 July 2021; revised 30 March 2022; accepted 26 May 2022; published 28 June 2022)

It has been proposed that an extended version of the Hubbard model which potentially hosts rich correlated physics may be well simulated by the transition metal dichalcogenide (TMD) moiré heterostructures. Motivated by recent reports of continuous metal-insulator transition (MIT) at half filling, as well as correlated insulators at various fractional fillings in TMD moiré heterostructures, we propose a theory for the potentially continuous MIT with fractionalized electric charges. The charge fractionalization at the MIT will lead to various experimental observable effects, such as a large resistivity as well as large universal resistivity jump at the continuous MIT. These predictions are different from previously proposed theory for interaction-driven continuous MIT. Physics in phases near the MIT will also be discussed.

DOI: 10.1103/PhysRevX.12.021067

Subject Areas: Condensed Matter Physics, Magnetism, Strongly Correlated Materials

I. INTRODUCTION

Many correlated phenomena have been observed in graphene-based moiré systems, such as high temperature superconductivity (compared with the bandwidth of the moiré bands), correlated insulators [1–9], and the strange metal phase [10,11], etc. The most fundamental reason for the emergence of these correlated physics is that the slow modulating moiré potential leads to very narrow bandwidths [12,13]. Great theoretical interests and efforts have been devoted to the graphene-based moiré systems [14–31]. But the theoretical description and understanding of the graphene-based moiré systems may be complicated by the fact that in the noninteracting limit the moiré minibands can have various types of either robust or fragile nontrivial topologies [32–40], although the exact role of the band topology to the interacting physics at fractional filling is not entirely clear. Hence similar narrow band systems with trivial band topology and unambiguous concise theoretical framework would be highly desirable. It was proposed that much of the correlated physics of the transition metal dichalcogenide (TMD) moiré heterostructure can be captured by an extended Hubbard model with an effective spin-1/2 electron on a triangular moiré lattice [41]:

$$H = \sum_{r,r',\alpha} -t_{r,r'} c^{\dagger}_{r,\alpha} c_{r',\alpha} + \text{H.c.} + \sum_{r} U n_{r,\uparrow} n_{r,\downarrow} + \cdots . \quad (1)$$

The electron operator $c_{r,\alpha}$ is constructed by states within a topologically trivial moiré miniband. Because of the strong spin-orbit coupling, the spin and valley degrees of freedom are locked with each other in the TMD moiré system. We will use $\alpha = \uparrow, \downarrow$ or 1,2 to denote two spin or equivalently two valley flavors. When a moiré band is partially filled, the correlated physics within the partially filled moiré minibands may be well described by Eq. (1), which only contains half of the degrees of freedom of a miniband in a graphene-based moiré system. The ellipsis in Eq. (1) can include further neighbor hopping, "spin-orbit" coupling terms allowed by symmetry [42], and further neighbor interaction. Note the spin-orbit coupling here refers to the hopping terms in Eq. (1) that depend on the spin index α and should not be confused with the bare spin-orbit coupling within the TMD system before the moiré superlattice is imposed. The TMD moiré systems are hence considered as a simulator for the extended Hubbard model on a triangular lattice [43].

Like the graphene-based moiré systems, the TMD moiré heterostructure is a platform for many correlated physics. This paper mainly concerns the metal-insulator transition (MIT) driven by interaction. The MIT of the Hubbard model on a triangular lattice has attracted much numerical effort recently [44,45]. The symmetry of the TMD moiré heterostructure is different from the simplest version of the Hubbard model; hence even richer physics can happen in the system. Continuous MIT has been reported at half

filling of the moiré bands (electron filling $\nu = 1/2$, or one electron per moiré unit cell on average) in the TMD moiré system [46,47]. The experimental tuning parameter of the MIT in the TMD heterostructure is the displacement field, i.e., an out-of-plane electric field, which tunes the width of the mini moiré bands, and hence the ratio between the kinetic and interaction energies in the effective Hubbard model. Correlated insulators have also been observed at various other fractional electron fillings, though the nature of the MITs at these fractional fillings have not been thoroughly inspected experimentally [48–51]. In this paper we mainly focus on $\nu = 1/2$, but other fractional fillings are also briefly discussed.

The nature of an interaction-driven MIT depends on the nature of the insulator phase near the MIT. The Hubbard model on the triangular lattice has one site per unit cell, which based on the generalized Lieb-Schultz-Matthis (LSM) theorem [52,53] demands that the insulator phase at half filling should not be a trivial incompressible (gapped) state which preserves the translation symmetry. If the insulator phase has a semiclassical spin order that breaks the translation symmetry, the evolution between the metal and insulator could involve two transitions: at the first transition a semiclassical spin order develops, which reduces the Fermi surface to several Fermi pockets; and at the second transition the size of the Fermi pockets shrink to zero, and the system enters an insulator phase. A more interesting scenario of the MIT only involves one single transition [54–56], but then the insulator phase is not a semiclassical spin order, instead it is a spin liquid state with a spinon Fermi surface. An intuitive picture for this transition is that, at the MIT, the charge degrees of freedom are gapped, but the spins still behave as if there is a "ghost" Fermi surface. The spinon Fermi surface can lead to the Friedel oscillation just like the metal phase [57]. The structure of the Fermi surface does not change drastically across the transition.

In a purely two-dimensional system, conductivity (or resistivity) is a dimensionless quantity; hence it can take universal value at the order of e^2/h (or h/e^2) in various scenarios. For example, the Hall conductivity of the quantum Hall state is precisely $\sigma_H = \nu e^2/h$; the conductivity (or resistivity) at a $(2+1)$D quantum critical point also takes a universal value at the order of e^2/h (or h/e^2) [58]. One central prediction given by the theory above for interaction-driven continuous MIT is that there is a universal resistivity jump at the order of $\sim h/e^2$ at the MIT compared with the metal phase, and the critical resistivity at the MIT should also be close to the order of h/e^2 (we review these predictions in the next section). In this paper we argue that the current experimental observations suggest that the nature of the MIT in $MoTe_2/WSe_2$ moiré superlattice without twisting [46] is beyond the previous theory [54–56], and we propose an alternative candidate theory of MIT with further charge fractionalizations. We will discuss how the alternative theory can potentially address the experimental puzzles, and more predictions based on our theory will be made. Our assumption is that the MIT in this system is indeed driven by electron-electron interaction (as was suggested by Ref. [46]): If the disorder plays the dominant role in this system, the MIT may be described by the picture discussed in Ref. [59].

The paper is organized as follows: In Sec. II we introduce an alternative parton construction for systems described by the extended Hubbard model with a spin-orbit coupling, which naturally leads to charge fractionalization at the interaction-driven MIT even at half filling. We also give an intuitive argument of physical effects caused by charge fractionalization at the MIT. In Sec. III, we discuss the theory for MIT when the insulating phase spontaneously breaks the translation symmetry. Section IV studies the theory of MIT when the insulating phase has different types of topological orders. In Sec. V we discuss various experimental predictions based on our theory, for the MIT and also the phases nearby. We present the details of our theory in Appendixes A–D, including the projective symmetry group, field theories, the calculation of dc resistivity, etc.

II. TWO PARTON CONSTRUCTIONS

The previous theory for the interaction-driven continuous MIT for correlated electrons on frustrated lattices was based on a parton construction. The parton construction splits the quantum number of an electron into a bosonic parton which carries the electric charge, and a fermionic parton which carries the spin. In this paper we compare two different parton constructions:

$$\text{I: } c_{\boldsymbol{r},\alpha} = b_{\boldsymbol{r}} f_{\boldsymbol{r},\alpha}, \qquad \text{II: } c_{\boldsymbol{r},\alpha} = b_{\boldsymbol{r},\alpha} f_{\boldsymbol{r},\alpha}. \tag{2}$$

In parton construction I only one species of charged bosonic parton b is introduced for electrons with both spin-valley flavors, while in parton construction II a separate charged bosonic parton b_α is introduced for each spin-valley flavor. As we will see later, the two different parton constructions will lead to very different observable effects. The construction I is the standard starting point of the theory of MIT that was used in previous literature [54–56]; construction II is usually unfavorable for systems with a full spin SU(2) invariance, because the parton construction itself breaks the spin rotation symmetry. But the construction II is a legitimate parton construction for the system under study, whose band structure in general does not have full rotation symmetry between the two spin-valley flavors.

The time-reversal symmetry of the microscopic TMD system relates the two spin-valley flavors. But it is not enough to guarantee a full SU(2) rotation symmetry between the two flavors. In fact, since the two flavors can be tied to the two valleys of the TMD material, the

trigonal warping of the TMD bands, which takes *opposite* signs for the two different valleys, can lead to the breaking of such an SU(2) rotation symmetry. To estimate the trigonal warping effect in the Hubbard model, one can compare the k^2 term and the $k_x^3 - 2k_x k_y^2$ term in the electron dispersion of one of the two layers in the heterostructure expanded at one valley. Then the relative strength of the trigonal warping compared to the SU(2)-invariant hopping in Eq. (1) is given by the ratio between the lattice constant of the original TMD material and that of the morié superlattice. In addition, the natural microscopic origin of the interactions in the Hamiltonian Eq. (1) is the Coulomb interaction between the electrons. The Coulomb interaction when projected to the low-energy bands relevant to the moiré-scale physics is expected to contain SU(2)-breaking interaction terms. The momentum conservation only guarantees the valley U(1) symmetry. Assuming the unscreened Coulomb interaction between electrons before the projection to the low-energy bands, further neighbor interaction will appear in the extended Hubbard model. The relative strength of the SU(2)-breaking interaction terms obtained from the projection compared to the SU(2)-invariant interactions can again be estimated by the ratio between the lattice constant of the original TMD material and the moiré superlattice, as the Fourier transform of unscreened Coulomb interaction in 2D space is $V_q \sim 1/q$.

The most important difference between these two parton theories resides in the filling of the bosonic partons. Since each bosonic parton carries the same electric charge as an electron, the total number of bosonic partons should equal to the number of electrons. Hence at electron filling ν (meaning 2ν electrons per unit cell), the filling factor of boson b in construction I is $\nu_b = 2\nu$, i.e., 2ν bosonic parton per unit cell; in construction II the filling factor of boson b_α has filling factor $\nu_b^\alpha = \nu$ for each spin-valley flavor. Hence even with one electron per site (half filing or $\nu = 1/2$ of the extended Hubbard model), the bosonic parton in construction II is already at half filling for each spin-valley flavor. The half filling will lead to nontrivial features inside the Mott insulator phase, as well as at the MIT. Another more theoretical difference is that in construction I there is one dynamical emergent U(1) gauge field a_μ which couples to both b and f_α, while in construction II there are two dynamical U(1) gauge fields $a_{\alpha,\mu}$, one for each spin-valley flavor.

In construction I, the bosonic parton b is at integer filling, and the MIT is naturally interpreted as a superfluid to Mott insulator (SF-MI) transition of boson b. At the MIT, using the Ioffe-Larkin rule [60], the dc resistivity of system is $\rho = \rho_b + \rho_f$, where ρ_b and ρ_f are the resistivity contributed by the bosonic and fermionic partons, respectively. ρ_f caused by disorder or interaction such as the umklapp process is a smooth function of the tuning parameter; the drastic change of ρ across the MIT arises from ρ_b. In the metal phase, i.e., the "superfluid phase" of b, ρ_b is zero, and the total resistivity is just given by ρ_f. Also, in the superfluid phase of b, the U(1) gauge field a_μ that couples to both b and f_α is rendered massive due to the Higgs mechanism caused by the condensate of b. In the insulator phase, ρ_b and ρ are both infinity, and the system enters a spin liquid phase with a spinon Fermi surface of f_α that couples to the dynamical U(1) gauge field a_μ. The MIT which corresponds to the condensation of b belongs to the 3D XY universality class. The dynamical gauge field a_μ is argued to be irrelevant at the transition due to the overdamping of the gauge field that arises from the spinon Fermi surface [55,56], and hence does not change the universality class of the SF-MI transition of b.

In parton construction I, at the MIT the bosonic parton contribution to the resistivity ρ_b is given by $\rho_b = Rh/e^2$, where R is an order-1 universal constant. In the order of limit $T \to 0$ before $\omega \to 0$, R is associated to the 3D XY universality class [61], because the gauge field a_μ is irrelevant as mentioned above. This universal conductivity at the 3D XY transition has been studied through various analytical and numerical methods [58,62–69]. At finite T and zero frequency, the gauge field a_μ can potentially enhance the value R to $R' > R$, based on a large-**N** calculation in Ref. [70] (**N** is different from N in our work). The evaluation in Ref. [70] gave $R' \sim 7.92$, while we evaluate the same quantity to be $R' \sim 7.44$. Hence the prediction of the construction I is that the dc resistivity of the system right at the MIT has a universal jump compared with the resistivity at the metallic phase close to the MIT [55,56]; i.e., $\Delta\rho = \rho_b = R'h/e^2$. With moderate disorder, at the MIT ρ_b of the bosonic parton is supposed to dominate the resistivity ρ_f of the fermionic parton f_α; hence the total resistivity $\rho = \rho_b + \rho_f$ should be close to ρ_b.

In the experiment on the $MoTe_2/WSe_2$ moiré superlattice, it was reported that disorder in the system is playing a perturbative role, and the continuous MIT is mainly driven by the interaction [46]. However, the reported resistivity ρ increases rapidly with the tuning parameter (the displacement field) near the MIT. The bare value of ρ near and at the MIT is significantly greater than h/e^2 (and significantly larger than the computed value of $\rho_b \sim R'h/e^2$ mentioned above), and it is clearly beyond the Mott-Ioffe-Regel limit; i.e., the system near and at the MIT is a very "bad metal" [71,72]. This suggests that the MIT is not a simple SF-MI transition of b, or in other words, b should be "much less conductive" compared with what was predicted in construction I considered in previous literature. We will demonstrate that construction II can potentially address the large resistivity at the MIT. The most basic picture is that, since b_1 and b_2 are both at half filling, the LSM theorem [52,53] dictates that the Mott insulator phase of each flavor of boson cannot be a trivial insulator; namely, the Mott insulator must either be a density wave that spontaneously breaks the translation symmetry or have topological order. In either case, the MIT is not a simple 3D XY transition, and

the most prominent feature of the transition is that the bosonic parton number (or the electric charge) must further fractionalize.

The MIT with charge fractionalization is discussed in detail in the next section using the dual vortex formalism, but the consequence of this charge fractionalization can be understood from a rather intuitive picture. Suppose b fractionalizes into N parts at the MIT, meaning the charge carriers at the MIT have charge $e_* = e/N$, then each charge carrier will approximately contribute a resistivity at the order of $h/e_*^2 \sim N^2 h/e^2$ at the MIT; and if there are in total N_b species of the fractionalized charge carriers, at the MIT the bosonic parton will approximately contribute resistivity,

$$\rho_b \sim \frac{N^2 h}{N_b e^2}. \tag{3}$$

There is a factor of N_b in the denominator because intuitively the total conductivity of b will be a sum of the conductivity of each species of fractionalized charge carriers, i.e., $\sigma_b = \sum_{j=1}^{N_b} \sigma_j$, in the unit of e^2/h (a more rigorous rule of combining transport from different partons will be discussed later). Hence, when $N^2/N_b > 1$, the construction II with inevitable charge fractionalization can serve as a natural explanation for the large ρ at the MIT, and it will also predict a large jump of resistivity $\Delta\rho$ at the MIT.

III. MOTT INSULATOR WITH TRANSLATION SYMMETRY BREAKING

A. General formalism

In this section, we discuss the MIT following the parton construction II discussed in the previous section. The MIT is still interpreted as the SF-MI transition of both spin-valley flavors of the bosonic parton b_α, although as we discussed previously the insulator cannot be a trivial incompressible state of b_α. In the superfluid phase of b_α, both U(1) gauge fields $a_{1,\mu}$ and $a_{2,\mu}$ that couple to the two flavors of partons are gapped out by the Higgs mechanism, and the system enters a metal phase of the electrons; b_1 and b_2 must undergo the SF-MI transition simultaneously, since the time-reversal or spatial reflection symmetries both interchange the two flavors of partons due to the spin-valley locking.

The dual vortex theory [73–75] is the most convenient formalism that describes a transition between a superfluid and a nontrivial insulator of a boson at fractional filling. If we start with a boson b, after the boson-vortex duality, a vortex of the superfluid phase of b becomes a point particle that couples to a dynamical U(1) gauge field A_μ, which is the dual of the Goldstone mode of the superfluid [not to be confused with the U(1) gauge field a_μ mentioned before that couples to the bosonic parton b]. In the dual picture, the superfluid phase of b (which corresponds to the metal phase of the electron) is the insulator phase of the vortex field, while the Mott insulator phase of b corresponds to the condensate of the vortices, which "Higgses" the U(1) gauge field A_μ, and drives the boson b into a gapped insulator phase. If at low energy there is only one component of vortex field with gauge charge 1 under A_μ (which corresponds to integer filling of boson b), the insulator phase of b is a trivial insulator without any further symmetry breaking or topological order; if there is more than one component of the vortex fields at low energy, or if the vortex field carries multiple gauge charges of A_μ, the insulator must be of nontrivial nature.

For example, when b has a fractional filling $\nu_b = 1/q$ with integer q, Refs. [76,77] studied the quantum phase transition between the bosonic SF and various MIs with commensurate density waves which spontaneously break the translation symmetry but have no topological order. The study is naturally generalized to filling factor $\nu_b = p/q$ with coprime integers (p, q). We can use this formalism in our system. Hereafter we focus on one spin-valley flavor α, and the index α will be hidden for conciseness. In this case the theory for the SF-MI transition at one spin-valley flavor is

$$\mathcal{L}^{(1)} = \sum_{j=0}^{N-1} [|(\partial_\mu - iA_\mu)\psi_j|^2 + r|\psi_j|^2] + u\left(\sum_{j=0}^{N-1} |\psi_j|^2\right)^2 + \frac{i}{2\pi} A \wedge d(a + eA_{\text{ext}}) + \cdots. \tag{4}$$

Here, ψ_j with $j \in \{0, \ldots, N-1\}$ are N flavors of vortex fields of the boson b at low energy, and A_μ is the dual gauge field of boson b: $[1/(2\pi)]dA = J_b$, where J_b is the current of boson b. a_μ is the gauge field that couples to both b and f, and A_{ext} is the external electromagnetic field. The reason there are N flavors of the vortex field is that the vortex which is defined on a dual honeycomb lattice will view the partially filled boson density as a fractional background flux of the dual gauge field A_μ through each hexagon, and the band structure of the vortex will have multiple minima in the momentum space. The degeneracy of the multiple minima is protected by the symmetry of the triangular lattice. ψ_j transforms as a representation of the projective symmetry group (PSG) of the lattice. Note that since Eq. (4) describes one of the two spin-valley flavors, the PSG that constrains Eq. (4) should include translation and $2\pi/3$ rotation of the lattice ($R_{2\pi/3}$). There is another more subtle symmetry $P_x\mathcal{T}$ for each spin-valley flavor of the boson and vortex fields. P_x that takes $x \to -x$ and time-reversal $\mathcal{T}$ both exchange the two spin-valley indices, but their product will act on the same spin-valley species, and part of its role is to take momentum k_y to $-k_y$.

In the Appendix B, we argue that P_y which takes y to $-y$ within each valley is also a good symmetry of the system, as long as valley mixing is negligible. One consequence of the P_y symmetry is that the expectation value of gauge flux

da can be set to zero for the theory Eq. (4), or equivalently the P_y symmetry ensures that the "chemical potential" term $\psi_j^* \partial_\tau \psi_j$ does not appear in Eq. (4), as P_y transforms a vortex to antivortex: $\psi_a \to U_{ab}\psi_b^*$. Also, with long moiré lattice constant, the trigonal warping $k_x^3 - 3k_x k_y^2$ in each valley of the original BZ of the system becomes less important compared with the leading-order quadratic dispersion expanded at each valley; hence the sixfold rotation $R_{\pi/3}$ becomes a good approximate symmetry of the effective Hubbard model with long moiré lattice constant.

The theory in Eq. (4) also has an emergent particle-hole symmetry. The simplest choice of the particle-hole symmetry is $\psi_a \to U_{ab}\psi_b^*$, $A \to -A$, $a \to -a$, and $A_{\text{ext}} \to -A_{\text{ext}}$. Although we used the same transformation matrix U_{ab} as P_y, this emergent particle-hole symmetry is different from P_y as it does not involve any spatial transformations. Note that any (spatially uniform) P_y-symmetric terms involving only the "matter fields" ψ_j must also preserve this emergent particle-hole symmetry. Another potentially relevant particle-hole symmetry-breaking perturbation that needs to be examined is given by the finite density of the fluxes dA. dA is tied to the physical U(1) charge density (compared to the charge density set by the fixed electron filling $\nu = 1/2$) and hence should have a vanishing spatial average. At the SF-MI transition point, the translation symmetry of the theory Eq. (4) and the fact that dA has a vanishing spatial average guarantee that dA has a vanishing expectation value everywhere, which respects the particle-hole symmetry. Therefore, the particle-hole symmetry is a valid emergent symmetry at the SF-MI critical point described by Eq. (4). The same argument would also conclude the emergent particle-hole symmetry at the ordinary SF-MI transition in the Bose-Hubbard model.

For parton construction II, when the electron has filling $\nu = 1/2$, both b_1 and b_2 are at filling $\nu_b^\alpha = 1/2$. For each flavor of b_α, the formalism in Ref. [77] would lead to a dual vortex theory with $N = 4$ components of vortex fields; i.e., there are four degenerate minima of the vortex band structure in the momentum space for each spin-valley index. This calculation is analogous to the frustrated Ising model on the honeycomb lattice [78,79]. Using the gauge choice of Fig. 1, the four minima are located at the K and K' points of the reduced Brillouin zone, with twofold degeneracy at each point.

B. From $N = 4$ to "$N = \infty$"

Reference [77] considered a specific band structure of the vortex, which only involved the nearest neighbor hopping of vortices on the dual honeycomb lattice. But there is no fundamental reason that further neighbor hopping of vortices should be excluded. Indeed, once we take into account further neighbor hopping, the dual vortex theory has a much richer possibility. We have explored the phase diagram of the dual vortex theory up to seventh neighbor hopping, and we obtained the phase diagram in Fig. 2(a). Further neighbor hopping of the vortex field can modify the band structure and lead to $N = 6$ or $N = 12$ components of vortex fields by choosing different hopping amplitudes. The $N = 6$ minima are located at three inequivalent M points of the reduced BZ (Fig. 2), each M point again has twofold degeneracy. The twofold degeneracy at each M point is protected by the translation symmetry of the triangular moiré lattice only, which is required by the LSM theorem. The shift of the vortex field minima from the K points to M points is similar to what was discussed in the context of frustrated quantum Ising models with further neighbor couplings [80,81]. With symmetries $T_{1,2}$, $R_{2\pi/3}$, and $P_x\mathcal{T}$ at each spin-valley flavor, the degeneracy of the $N = 6$ minima at the M points are protected.

There are two regions in the phase diagram in Fig. 2(b) with $N = 12$ modes of vortex, two at each momentum.

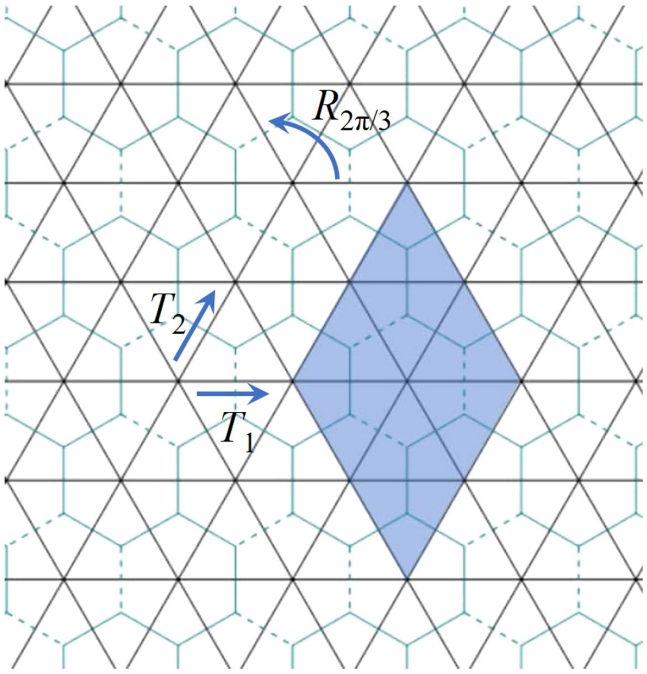

FIG. 1. The triangular moiré lattice, and its dual honeycomb lattice. In the parton construction II, the bosonic parton b_α is at half filling for each spin-valley flavor, which becomes a π flux of the dual gauge field A_μ through the hexagon of the dual honeycomb lattice. Hence the vortex ψ defined on the dual honeycomb lattice does not have a uniform hopping amplitude; the dashed links on the dual honeycomb lattice have negative hopping amplitudes. The symmetry of the lattice will be realized as a projective symmetry group. There are eight dual sites per unit cell (shaded area) in this gauge choice. At each spin-valley flavor, there are translation symmetries $T_{1,2}$, a rotation symmetry $R_{2\pi/3}$, and a product of reflection $P_x(x \to -x)$ and time reversal $\mathcal{T}$. We also argue that P_y is a symmetry of the system as long as there is no valley mixing, and the sixfold rotation $R_{\pi/3}$ becomes a good approximate symmetry of the Hubbard model in the case of long moiré lattice constant.

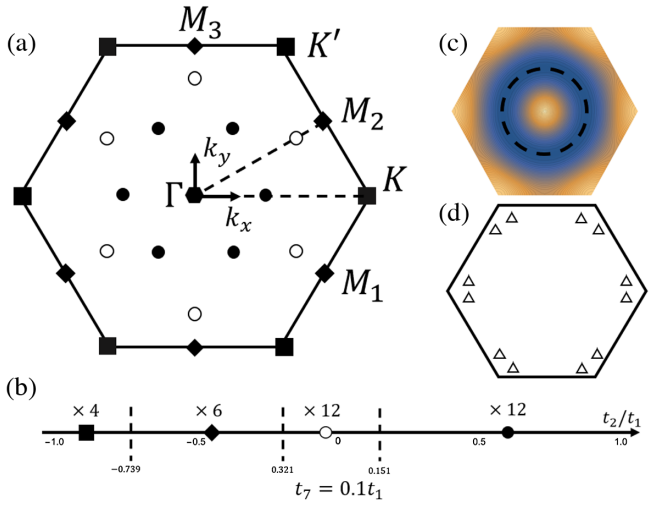

FIG. 2. (a) The minima of the vortex band structure. With nearest neighbor vortex hopping on Fig. 1, the minima locate at the K and K' points of the Brillouin zone, each K point has two fold degeneracy; with further neighbor hoppings, the minima can shift to the three M points, still with twofold degeneracy at each M point. (b) The phase diagram of vortex modes with seventh neighbor hopping $t_7 = 0.1t_1$, and by tuning t_2 there are two regions in the phase diagram with $N = 12$ vortex modes at low energy. The 12 vortex modes are located on the lines between either Γ and K/K' or Γ and M. (c) With only t_1 and t_2, there is a large region of the phase diagram where there is a ring degeneracy of the vortex band structure. (d) All the symmetries (including approximate symmetries) of the system can protect up to 24 degenerate vortex modes, which locate at 12 incommensurate momenta in the BZ.

The six incommensurate momenta at the minima of the vortex band structure can be located either on the lines between Γ and K/K' or Γ and M. With the $R_{\pi/3}$ symmetry that becomes a good approximate symmetry with long moiré lattice constant, the degeneracy of the $N = 12$ vortex modes is protected. In principle, all the symmetries together including $R_{\pi/3}$ can protect up to $N = 24$ degenerate minima, as shown in Fig. 2(d).

For a theory with N components of vortex fields, the electric charge carried by the boson b will fractionalize. Under the boson-vortex duality $[1/(2\pi)]dA = J_b$, the boson number of b becomes the flux number of the dual gauge field A_μ. The gauge flux of A_μ is trapped at the vortex core of each field ψ_j (we denote the vortex of ψ_j as φ_j). With N components of the vortex fields, the vortex of each ψ_j field will carry $1/N$ flux quantum of the gauge field A_μ; hence the charge e_* of each fractionalized charge carrier should be e/N at the MIT. And there are in total $N_b = 2N$ species of the charge carriers (the factor of 2 comes from the two spin-valley flavors).

With just t_1 and t_2 (first and second neighbor vortex hopping), there is a large region of the parameter space where the minima of the vortex band structure form a ring. This one-dimensional ring degeneracy is not protected by the symmetry of the system, but its effect may still be observable for a finite energy range. A ring degeneracy is analogous to $N = \infty$ in Eq. (4). Condensed matter systems with a ring degeneracy have attracted considerable interests [82–85]. By integrating out the vortices with ring degeneracy, a "mass term" for the transverse component of A_μ is generated in the infrared limit [85] (in the limit of momentum going to zero before frequency), meaning the fluctuation of A_μ is highly suppressed, which is consistent with the intuition of $N = \infty$.

The ellipsis in Eq. (4) includes other terms allowed by the PSG of the triangular lattice, but break the enlarged flavor symmetry of the CP^{N-1} model field theory. More details about PSG, extra terms in the Lagrangian, coupling to fermionic parton f_α [86], and the possible valence bond solid orders with $N = 6$ are discussed in Appendixes A and B. The exact fate of the critical theory in the infrared is complicated by these extra perturbations. It was shown previously that nonlocal interactions can drive a transition to a new fixed point [87–89], and here nonlocal interactions arise from coupling to the fermionic partons [86]. Hence the transition may eventually flow to a CFT different from the CP^{N-1} theory in Eq. (4), or be driven to a first-order transition eventually. But as long as the first-order nature is not strong, the charge fractionalization and large resistivity discussed in the next section is expected to hold at least for a considerable energy-temperature window.

So far we have not paid much attention to the dynamical gauge fields a_μ in parton construction I or $a_{\alpha,\mu}$ in construction II shared by the bosonic and fermionic partons, as the gauge coupling between b (b_α) and the gauge field is irrelevant at the MIT with a background spinon Fermi surface. Here we briefly discuss the fate of the spinon Fermi surface in the insulator phase. When the bosonic parton b is gapped, the theory of spinon Fermi surface coupled with the dynamical U(1) gauge field is a problem that has attracted a great deal of theoretical efforts [90–96]. These studies mostly rely on a "patch" theory approximation of the problem, which zooms in one or two patches of the Fermi surface. Then an interacting fixed point with a nonzero gauge coupling is found in the IR limit based on various analytical perturbative expansion methods.

Previous studies have also shown that the non-Fermi liquid obtained through coupling a Fermi surface to a dynamical bosonic field can be instable against BCS pairing of fermions [97–103]. If there is only one flavor of U(1) gauge field, the low-energy interacting fixed point is expected to be robust against this pairing instability, because the U(1) gauge field leads to repulsive interaction between the spinons. However, when there are two flavors of U(1) gauge fields [103,104], like the case in our parton construction II, the two U(1) gauge fields can lead to interflavor spinon pairing instability. This interflavor pairing can still happen at the MIT. But depending on the

microscopic parameters this instability can happen at rather low-energy scale.

C. Resistivity at the MIT

For low frequency and temperature, the resistivity of a system is usually written as $\rho(x)$ with $x = \omega/T$. The dc conductivity at zero temperature corresponds to $x = 0$, i.e., the limit $\omega \to 0$ before $T \to 0$. As we have mentioned, the interaction-driven MIT has a jump of resistivity at the MIT compared with the metal phase near MIT, and this jump is given by the resistivity ρ_b of the bosonic parton b_α. For a bosonic system with an emergent particle-hole symmetry in the infrared, $\rho_b(x)$ with $x = 0$ or $x = \infty$ have attracted most studies. In general, both $\rho_b(0)$ and $\rho_b(\infty)$ should be universal numbers at the order of $\sim h/e^2$. The reason $\rho_b(0)$ could be finite even without considering disorder and umklapp process is that, with an emergent particle-hole symmetry in the infrared discussed in the previous section, there is zero overlap between the electric current and the conserved momentum density (extra subtleties about this from hydrodynamics are discussed in Sec. VI). The universal $\rho_b(0)$ was evaluated in Ref. [70] for the interaction-driven MIT without charge fractionalization. The calculation therein was based on Boltzmann equation in a theoretical large-**N** limit and eventually **N** was taken to 1 (we remind the readers that the **N** introduced in Ref. [70] was for technical reasons; it is not to be confused with N used in this work).

We have generalized the computation in Ref. [70] to our case with N components of vortex fields and charge fractionalization. To proceed with the computation we need to turn on "easy-plane" anisotropy to Eq. (4) and perform duality to the basis of fractional charge carriers φ_j [Eq. (C5)]. The φ_j will be coupled to multiple gauge fields which are the dual of the ψ_j fields. Eventually the total resistivity $\rho_b(0)$ is obtained through a generalized Ioffe-Larkin rule, which combines the resistivity of each parton φ_j into ρ_b:

$$\rho_b = \frac{\hbar}{e^2}\left(\sum_{j=0}^{N-1}\rho_{b,j}\right). \tag{5}$$

$\rho_{b,j}$ is the resistivity of each charge carrier φ_j when its charge is taken to be 1. The detail of the computation is presented in the Appendix D, and we summarize the results here. For N flavors of vortices in Eq. (4), the resistivity $\rho_b(0)$ at the MIT roughly increases linearly with N, as was expected through the intuitive argument we gave before:

$$\rho_b(0) = \Delta\rho = [R^{(0)} + R^{(1)}(N-1)]\frac{h}{e^2}, \tag{6}$$

where $R^{(0)} \sim 3.62$, $R^{(1)} \sim 1.68$. We would like to compare our prediction with the previous theory of MIT without charge fractionalization. In the previous theory, the dc resistivity jump is evaluated to be $\Delta\rho \sim 7.92h/e^2$ [70] (we reproduced this calculation and our result at $N = N_b = 1$ is $7.44h/e^2$). Equation (3) suggests that when $N \geq 4$, the resistivity jump in our case is indeed larger than that predicted by the previous theory of MIT.

We would also like to discuss the ac resistivity $\rho_b(\infty)$. One way to evaluate $\rho_b(\infty)$ is to again start with Eq. (C5), and follow the same strategy as the calculation of the dc resistivity. According to the generalized Ioffe-Larkin rule, the ac resistivity contributed by *each valley* is given by

$$\rho_b = N\frac{1}{\sigma_\varphi}\frac{\hbar}{e^2}, \qquad \sigma_\varphi = \lim_{\omega\to 0}\frac{1}{i\omega}\langle J^\varphi_\omega J^\varphi_{-\omega}\rangle_{\vec{p}=0}, \tag{7}$$

where $J^\varphi = i\varphi_j^*\nabla\varphi_j + \text{H.c.}$ is the current of the charge carrier φ_j. With the theoretical large-**N** limit mentioned above, the effects of all the dynamical gauge fields are suppressed, and φ_j will contribute conductivity $\sigma_\varphi(\infty) = \frac{1}{16}$ [contrary to dc transport, $\sigma_\varphi(\infty)$ does not need collisions; the effects of dynamical gauge fields can be included through the $1/\mathbf{N}$ expansion]. Eventually one would obtain resistivity from each valley,

$$\rho_b = \frac{8N}{\pi}\frac{h}{e^2}; \tag{8}$$

the final resistivity of the system is half of Eq. (8) due to the two spin-valley flavors. With $N = 1$, the transition should belong to the ordinary 3D XY universality class, and the value given by Eq. (8) is not far from what was obtained through more sophisticated methods (see, for instance, Refs. [63–65], $\rho_b \sim 2.8h/e^2$). This should not be surprising as the 3D XY universality class can be obtained perturbatively from the free-boson theory. In our current case with charge fractionalization, with $N \geq 4$, the total ac resistivity which is half of the value in Eq. (8) is larger than the universal resistivity at the 3D XY transition.

Another way to evaluate the resistivity of Eq. (4) is by integrating out ψ_j from Eq. (4), and an effective Lagrangian for A_μ is generated:

$$\mathcal{L} = \sum_{p_\mu}\frac{Np}{16}\left(\delta_{\mu\nu} - \frac{p_\mu p_\nu}{p^2}\right)A_\mu(p)A_\nu(-p). \tag{9}$$

This effective action is supposed to be accurate in the limit of $N \to \infty$. The electric current carried by b is $J^b = (e/2\pi)dA$; hence the current-current correlation can be extracted from the photon Green's function based on the effective action Eq. (9):

$$\rho_{b,N\to\infty} = \frac{\pi N}{8}\frac{h}{e^2}. \tag{10}$$

Again the final resistivity of the system is half of Eq. (10) due to the two spin-valley flavors. The evaluation Eq. (10) is still proportional to N just like Eq. (8). These two

different evaluations discussed above give different values for $N = N_b = 1$, and compared with the known value of the universal resistivity at the 3D XY transition, the evaluation in Eq. (8) is much more favorable, though the evaluation Eq. (10) based on Eq. (9) is supposed to be accurate with large N.

When there is a ring of degeneracy in the vortex band structure, as we mentioned before the gauge field A_μ will acquire a "mass term" after integrating out ψ_j [85]. In this case the resistivity of the system at the MIT will be infinity, as the dynamics of A_μ is fully suppressed by the mass term in the infrared. One can also integrate out the action of A_μ with the mass term, and verify that the response theory of $A_{\rm ext}$ is no different from that of an insulator in the infrared limit. This is consistent with both Eqs. (8) and (10) by naively taking N to infinity. In Ref. [85] when the boson field has a ring degeneracy, the phase is identified as a Bose metal; this is because in Ref. [85] it is the boson with ring degeneracy that carries charges. But in Eq. (4) the electric charge is carried by the flux of A_μ.

IV. MOTT INSULATOR WITH TOPOLOGICAL ORDER

As we explained in the previous section, due to the fractional filling of boson b_α, the vortex dynamics is frustrated by the background fractional flux through the hexagons. To drive the system into an insulator phase, the vortex can either condense at multiple minima in the BZ, as was discussed in the previous section, or form a bound state that carries multiple gauge charge of A_μ and become "blind" to the background flux. In parton construction II, with electron filling $\nu = 1/2$, each flavor of boson is at filling $\nu_b = 1/2$. The double vortex, i.e., bound state of two vortices, or more generally the bound state of N vortices with even integer N, no longer sees the background flux. Hence the N vortex can condense at zero momentum, and its condensate will drive the system into a Z_N topological order.

After the boson-vortex duality, the theory for the N-vortex condensation at one of the two spin-valley flavors is

$$\mathcal{L}^{(2)} = |(\partial_\mu - iNA_\mu)\psi|^2 + r|\psi|^2 + g|\psi|^4 + \frac{i}{2\pi} A \wedge d(a + eA_{\rm ext}) + \cdots . \tag{11}$$

The condensate of ψ will break the U(1) gauge field to a Z_N gauge field, whose deconfined phase has a nontrivial Z_N topological order. In the Z_N topological order as well as at the MIT, the charge carrier is an anyon of the Z_N topological order, and it carries charge $e^* = e/N$. We still label the fractional charge carrier as φ. φ carries charge e/N, and is coupled to a Z_N gauge field originated from the Z_N topological order discussed in the previous paragraph.

In our case, in order to preserve the time-reversal symmetry, both spin-valley flavors should form a Z_N topological order simultaneously. Hence there is one species of φ_α field for each spin-valley flavor. The MIT can equally be described as the condensation of the φ_α field, and since the Z_N gauge field does not lead to singular correction in the infrared, the condensation of φ_α is a 3D XY^* transition, and the transition for $N = 2$ was discussed in Refs. [53,105–109]. The b_α field is now a composite operator of φ_α. In the condensate of φ_α, the electron operator c_α is related to the fermionic parton operator f_α through $c_\alpha \sim \langle b_\alpha \rangle f_\alpha \sim \langle \varphi_\alpha^N \rangle f_\alpha$. The coupling between the two flavors of φ_α, i.e., the coupling $|\varphi_1|^2|\varphi_2|^2$, is irrelevant at the decoupled 3D XY^* transition according to the known critical exponents of the 3D XY^* transition. There are also couplings such as $|\varphi_\alpha|^2 f_\alpha^\dagger f_\alpha$ allowed by all the symmetries, but after formally integrating out the fermions, the generated couplings for φ_α are also irrelevant at the two decoupled 3D XY^* universality classes. The reason is that after formally integrating out the fermions, terms such as $(|\omega|/q)|\varphi_\alpha|^2_{\omega,\vec{q}}|\varphi_\beta|^2_{-\omega,-\vec{q}}$ can be generated, but this term is irrelevant knowing that the standard critical exponent $\nu > 2/3$ for the 3D XY^* transition.

Following the large-$\mathbf{N}$ calculation discussed before, the dc resistivity jump $\rho_b(0)$ would be $N^2/2$ times that of the previous theory [70]; namely,

$$\rho_b(0) \sim R^{(2)} N^2 \frac{h}{e^2}, \tag{12}$$

where $R^{(2)} = R'/2 \sim 3.7$ based on our evaluation. The ac jump at the MIT is enhanced by the same factor compared with the previous theory. We also note that the fractional universal conductivity at the transition between the superfluid and a Z_2 topological order was observed numerically in Ref. [109].

Another set of natural topological orders a boson at fractional filling can form is bosonic fractional quantum Hall (BFQH) states which are close analogs to the bosonic Laughlin's wave function. We would like to discuss this possibility as a general exploration, although this state breaks the P_y symmetry (but it still preserves the product $P_x\mathcal{T}$ symmetry). If we interpret the half-filled boson at each site as a quantum spin-1/2 system, this set of states is analogous to a chiral spin liquid [110,111]. The Chern-Simons (CS) theory for this set of states at each valley reads

$$\mathcal{L}_{\rm cs} = -\frac{ik}{4\pi} A \wedge dA + \frac{i}{2\pi} A \wedge d(a + A_{\rm ext}), \tag{13}$$

with an even integer k and a dynamical Spin_c U(1) gauge field A. The topological order characterized by this theory is the $\mathrm{SU}(k)_1$ topological order. Here, the integer k needs to be even so that this theory is compatible with the LSM constraint imposed by the boson filling 1/2 on the lattice

[112]. This is because the boson filling $1/2$ requires the topological phase to contain an Abelian anyon that carries a fractional charge $1/2$ (modulo integer). There should be one such anyon per unit cell to account for the boson filling $1/2$ on the lattice. The fact that such an anyon carries a fractional charge $1/2$ implies that this anyon should generate under fusion an Abelian group $\mathbb{Z}_p$ with p an even number. Such a fusion rule is incompatible with any odd value of k. Therefore, k needs to be even in the theory given by Eq. (13). The time reversal of the TMD moiré system demands that the bosonic parton b_α with opposite spin-valley index α forms a pair of time-reversal conjugate BFQH states. Or in other words, if we take both spin-valley flavors together, this state is a fractional topological insulator, like the state discussed in Ref. [113].

The MIT is now a direct transition between the BFQH state and the superfluid of b_α. When the even integer k is $k = 2n^2$ with odd integer n, there is a natural theory for this direct continuous transition, and its simplest version with $n = 1$ was proposed in Ref. [114]. The transition is a 3D QED with two flavors of Dirac fermions coupled to the dynamical U(1) Spin_c gauge field A_μ (the dual of the Goldstone mode of the boson superfluid) with a Chern-Simons term at level n^2, and the fermions have gauge charge n:

$$\mathcal{L}^{(3)} = \sum_{j=1}^{2} \bar{\chi}_j \gamma \cdot (\partial - inA)\chi_j + M\bar{\chi}_j\chi_j - \frac{in^2}{4\pi} A \wedge dA + \frac{i}{2\pi} A \wedge d(a + eA_{\text{ext}}) + \cdots . \tag{14}$$

In this theory, the fact that A is a Spin_c U(1) gauge field and that n is odd guarantees that this theory describes the phases of a boson. A Spin_c connection A_μ means a U(1) gauge field with a "charge-statistics relation": there is no fermionic object that is neutral under A_μ. When A_μ is a Spin_c U(1) gauge field, and n is an odd integer in Eq. (14), Eq. (14) describes an interacting state of bosons that carries electric charge e. The charge-e object of Eq. (14) that is also neutral under A_μ is a composite of 2π flux of A_μ and n fermions χ. This composite is a boson as long as n is an odd integer, and this composite should be identified as b_α in Eq. (2). The ellipsis in this Lagrangian includes other terms such as the Maxwell term of the gauge field A_μ. Note that this equation is for one of the two spin-valley flavors of the physical system. The mass M of the Dirac fermions is the tuning parameter of the transition. With one sign of the mass term, after integrating out the Dirac fermions, the Spin_c U(1) gauge field A will acquire a Chern-Simons term at level $-2n^2$, which describes the $\text{SU}(k)_1$ topological order with $k = 2n^2$. With the opposite sign of M, there is no Chern-Simons term of the gauge field A after integrating out the Dirac fermions, and the Maxwell term of the gauge field A is the dual description of the superfluid phase. Hence by tuning M the system undergoes a transition between the $k = 2n^2$ BFQH state and the superfluid state of b (the metal phase of the original electron system).

The translation symmetry of the system actually guarantees that the two flavors of Dirac fermions are degenerate in Eq. (14). If these two Dirac fermions are not degenerate, an intermediate topological order is generated by changing the sign of the mass of one of the Dirac fermions in Eq. (14). Then after integrating out the fermions, the gauge field A acquires a total CS term with an odd level $-n^2$, which violates the LSM constraint imposed by the boson filling $1/2$. Therefore, the masses of the two flavors of the Dirac fermions in Eq. (14) should be the same. In fact, for the simplest case with $n = 1$ ($k = 2$), an explicit parton construction of this transition can be given following the strategy in Ref. [114], and the two Dirac fermions in Eq. (14) are two Dirac cones of a π-flux state of χ on the triangular lattice. The degeneracy of these two Dirac fermions is protected by the translation symmetry of the triangular lattice. From the parton formalism one can also see that the boson b is constructed as a product of the two fermions χ_i.

At the transition $M = 0$, though it is difficult to compute the resistivity of Eq. (14) exactly, the resistivity $\rho(x)$ should scale as $1/k$ with large $k \sim n^2$, as after integrating out χ_j the entire effective action of A scales linearly as k. Then after integrating out A, the response theory to A_{ext} is proportional to $1/k$.

V. SUMMARY OF PREDICTIONS

So far we have discussed three different kinds of possible Mott insulators at half filling of the extended Hubbard model, based on the parton construction II: (1) Mott insulators with translation symmetry breaking, (2) a Z_N topological order at each spin-valley flavor with even integer $N \geq 2$, and (3) a pair of conjugate BFQH states at two spin-valley flavors. For all scenarios, we have evaluated the bosonic parton contribution to the resistivity ρ_b at the MIT, which is also the universal jump of resistivity $\Delta\rho$. The predicted resistivity jump for the three scenarios are summarized in Table I.

Another observable effect predicted by the previous theory of interaction-driven MIT is the scaling of quasiparticle weight $\sqrt{Z}$ near the MIT [55,56], where $\sqrt{Z} \sim r^{\beta_1} \sim |r|^{0.33}$. Our theory also gives a different

TABLE I. Summary of resistivity for three scenarios considered in this work. TO is topological order.

Nature of insulator	$\Delta\rho$, or ρ_b
(1) Density wave	$\rho_b(0) \sim [R^{(0)} + R^{(1)}(N-1)](h/e^2)$
(2) Z_N TO each flavor	$\rho_b(0) = R^{(2)}N^2(h/e^2)$
(3) Conjugate BFQH	$\rho_b(x) \sim (1/k)(h/e^2)$

prediction of the quasiparticle weight compared with the previous theory, and this is most conveniently evaluated for scenario (2). In the metal phase but close to the MIT, the quasiparticle weight scales as

$$\sqrt{Z} \sim \langle \varphi_\alpha^N \rangle \sim |r|^{\beta_N}, \tag{15}$$

where $\beta_N = \nu \Delta_N$. $\nu \sim 0.67$ is the standard correlation length exponent at the 3D XY^* transition (it is the same as the 3D XY transition) and Δ_N is the scaling dimension of φ^N at the 3D XY transition. These exponents can be extracted from numerical simulation on the 3D XY and XY^* transitions. For example, when $N = 2$, β_2 should be close to 0.8 [105,106,115]; hence, $\sqrt{Z} \sim |r|^{0.8}$. The scaling of quasiparticle weight can be checked in future experiments through the measurement of local density of states of electrons.

For scenario (1), i.e., where the insulator has translation symmetry breaking, the scaling of quasiparticle weight can be estimated with large N in Eq. (4). The boson creation operator $b^\dagger$ is a monopole operator of A_μ which creates a 2π gauge flux. With large N in Eq. (4) the monopole operator has scaling dimension proportional to N [116,117]; hence the critical exponent β in the quasiparticle weight $\sqrt{Z} \sim |r|^\beta$ is expected to be proportional to N. The similar evaluation applies to Eq. (14), and the creation operator $b^\dagger$ has a scaling dimension proportional to k, which is also proportional to $\sqrt{Z}$.

As we explained, our theory provides a natural explanation of the anomalously large resistivity at the MIT. Another qualitative experimental feature reported in Ref. [46] is that the resistivity drops rapidly as a function of temperature at the MIT where the charge gap vanishes. Our theory also provides a natural explanation for the temperature dependence of the critical resistivity. At zero temperature the bosonic chargeon parton b fractionalizes into multiple partons with smaller charges, and these partons will couple to extra gauge fields. These extra gauge fields will all confine at finite temperature. Hence at finite temperature, there is a crossover from transport with fractionalized charge to unfractionalized charge, which will cause a significant drop of resistivity with increasing temperature.

In the following paragraphs we discuss physics in phases near the MIT, based on our theory. These analyses can distinguish the three possible scenarios discussed to this point. Let us first discuss the insulator phase at fixed electron filling $\nu = 1/2$. The scenario (3) describes a topological order that is essentially a topological fractional quantum spin Hall insulator; hence this insulator phase, if it does exist, must have nonchiral gapless modes localized at the boundary of the system. These nonchiral edge states should lead to similar experimental phenomena as the experiments on quantum spin Hall insulator [118], but rather than edge conductance $2e^2/h$, the edge conductance of the fractional quantum spin Hall insulator should be $2e^2/(kh)$, which is twice that of the edge conductance of the BFQH state with CS level k. Also, the edge conductance should be suppressed by an external magnetic field, also analogous to what was observed in Ref. [118].

The insulating phase of scenario (1) and scenario (2) also lead to distinctive predictions. In scenario (1), the electric charges are only deconfined at the MIT, but still confined in the insulating phase, which has no topological order. Hence the charge deconfinement of scenario (1) is analogous to the original deconfined quantum critical point discussed in Refs. [107,108]. The confinement of fractional charges in scenario (1) happens even at zero temperature in the insulating phase. However, in scenario (2), the insulator phase has a Z_N topological order that supports deconfined fractional charge at zero temperature even in the insulator phase. While at finite temperature, the Z_N gauge field will lead to confinement of fractional charges with confinement length $\xi \sim \exp(c\Delta_m/T)$, where Δ_m is the gap of the fractionalized Z_N gauge fluxes, which is an anyon with nontrivial statistics with the fractional charges. If we look at the insulator phase close to the MIT, the gap of the fractional charge (the e anyon of the Z_N topological order) is supposed to be smaller than Δ_m, as the MIT corresponds to the condensation of the e anyon; hence at very low temperature the thermally activated e anyon has a much smaller distance l_e with each other compared with ξ. Then at low but finite temperature the transport is governed by charge carriers with gap Δ_e and charge $e_* = e/N$. The gap Δ_e can be extracted from fitting the low-temperature transport data versus temperature. However, if one measures the tunneling gap through tunneling spectroscopy, since the external device can only inject a single electron which fractionalizes into multiple e anyons, the tunneling gap should be approximately $N\Delta_e$. This contrast between tunneling gap and the thermally activated transport gap happens in scenario (2) but not scenario (1).

We also consider the metallic phase next to the insulator after charge doping, and we will see that scenario (2) also leads to very nontrivial predictions due to the deconfined nature of the Z_N topological order. In scenario (2), after some charge doping, we expect a metallic state with charge fractionalization at low temperature. The bosonic charge carriers are coupled to the Z_N gauge field as well as the U(1) gauge field a_μ that are shared with the fermionic partons f_α. When the temperature is increased, the Z_N gauge field will confine, and due to the time-reversal symmetry, the confine-deconfine crossover should happen for both spin and valley flavors simultaneously. In the following, we shall only focus on one spin or valley. According to the Ioffe-Larkin composition rule, the total resistivity is composed of contributions from both bosonic and fermionic partons $\rho = \sigma^{-1} = \sigma_b^{-1} + \sigma_f^{-1}$. Let us assume

the resistivity of both the bosonic and fermionic sectors are dominated by the scattering with the gauge field a_μ (this of course assumes that the momentum of the gauge field a_μ can relax through other mechanisms such as disorder). This scattering mechanism was first evaluated in Ref. [119]. The gauge-field propagator can be written as $D(\omega,\boldsymbol{q})^{-1} = i\gamma\omega/q + \chi_d q^2$, where the ω/q term is due to the Landau damping from the Fermi surface, and the "diamagnetic" χ_d is roughly a constant within the temperature window of interest. The scattering rate can then be estimated using the imaginary part of the boson or fermion self-energy:

$$\mathrm{Im}\Sigma_{b,f}(\omega,\boldsymbol{k}) = \int_0^\infty d\omega' \int \frac{d^2\boldsymbol{k}'}{(2\pi)^2}[1+n_b(\omega')][1\pm n_{b,f}(\omega_{\boldsymbol{k}'})]\frac{(k_\alpha+k'_\alpha)(k_\beta+k'_\beta)}{2m_{b,f}}\frac{\delta_{\alpha\beta}-q_\alpha q_\beta}{\boldsymbol{q}^2}\delta(\omega-\omega_{\boldsymbol{k}'}-\omega')\mathrm{Im}D(\omega',\boldsymbol{q}),$$

where $\boldsymbol{q}=\boldsymbol{k}'-\boldsymbol{k}$, $n_{b,f}(\omega)$ denotes the Bose-Einstein (Fermi-Dirac) distribution function, and $m_{b,f}$ is the boson-fermion mass. We must stress that the expression of $\Sigma_{b,f}$ is valid for partons with gauge charge 1. When the Z_N gauge field is deconfined, each boson carries the gauge charge $1/N$ of the gauge field a_μ, and therefore there is an additional factor $1/N^2$ in the self-energy. The integral was evaluated in Ref. [119], and the timescale responsible for transport has an extra factor proportional to q^2 in the integral. After taking these into account, we obtain the "transport" scattering rate for boson or fermion

$$\frac{1}{\tau_f}\sim T^{4/3}, \qquad \frac{1}{\tau_b}\approx\frac{k_B T}{m_b\chi_d}. \tag{16}$$

Comparing $1/\tau_b$ and $1/\tau_f$, we can see that the resistivity is dominated by the boson-gauge scattering at low temperature, and the bosonic partons are in a disordered phase rather than a quasi-long-range order at finite temperature due to their coupling to the dynamical gauge field a_μ. We take the Drude formula for the dilute Bose gas that we use to model the bosonic partons at finite temperature:

$$\rho\sim\frac{m_b}{n_* e_*^2}\frac{1}{\tau_b}\sim\frac{g_*^2}{n_* e_*^2}\frac{k_B T}{\chi_d}, \tag{17}$$

where $e_*=e/N$ and $g_*=1/N$ denote the electric and gauge charges of bosons, and $n_* e_*$ is the doped physical electric charge density. Here, we have assumed that the resistivity ρ is dominated by the boson contribution because (i) the scattering rate of the boson is bigger compared to the fermions at low temperature as shown in Eq. (16) and (ii) the bosons have much lower density at low charge doping compared to the fermions which already have finite Fermi surface at zero charge doping. In the following discussion, we work under these assumptions at least up to the temperature scale T_c around which the Z_N gauge becomes fully confined.

The Z_N gauge field is fully confined when ξ is at the same order as the lattice constant; i.e., $T>T_c\sim\Delta_m$. Here we assume that the gauge field a_μ that is coupled to the fermionic parton is less prone to confinement due to its coupling to the large density of gapless fermions. Above T_c, the charge carriers in the system carry charge e. The equation above still holds with the substitutions $e_*\to e=Ne_*, g_*\to g=Ng_*, n_*\to n=n_*/N$. We expect there is a crossover from the deconfined value of resistivity $\rho(T\sim 0)$ to the confined value $\rho(T\geq T_c)$:

$$\frac{(d\rho/dT)_{T\geq T_c}}{(d\rho/dT)_{T\sim 0}}\sim N. \tag{18}$$

This is an observable effect of scenario (2) that can be experimentally verified. Note that the crossover caused by confinement at the metallic phase is different from the critical point of the MIT, as transport at the critical point originates from rather different physics; for example, both particles and holes will contribute to the charge transport at the critical point [120].

Contrary to the Ioffe-Larkin rule, the total thermal conductivity of the system is a sum of the contribution from the bosonic parton, fermionic parton, and also the gauge boson. With low charge doping away from $\nu=1/2$, we expect the fermionic partons dominate the thermal transport according to Ref. [121]: $\kappa_f\sim T^{1/3}$. As we discussed above, in scenario (2) the low-temperature charge transport is dominated by the boson contribution $\sigma_b\sim 1/T$, while the thermal transport is dominated by the fermion contribution $\kappa_f\sim T^{1/3}$. Because of the crossover of charge transport at finite temperature caused by the confinement of the Z_N gauge field in scenario (2), there is also an observable prediction one can make for the Lorentz number $L=\kappa/(T\sigma)\approx\kappa_f/(T\sigma_b)$:

$$\frac{(L/T^{1/3})_{T\geq T_c}}{(L/T^{1/3})_{T\sim 0}}\sim N. \tag{19}$$

VI. SUMMARY, DISCUSSION, AND OTHER FRACTIONAL FILLINGS

In this work we proposed a theory for a potentially continuous metal-insulator transition for the extended Hubbard model on the triangular lattice at half filling

(one electron per unit cell). The extended Hubbard model is simulated by the TMD moiré systems. We introduce a different parton construction from the previous literature, which leads to a series of observable predictions. We demonstrated that our theory is more favorable given the current experiments on the heterobilayer TMD moiré systems. Although our theory was motivated by the recent experiments on $MoTe_2/WSe_2$ moiré superlattice [46], we envision our theory can have broad application given the recent rapid progresses in synthesizing pure two-dimensional systems.

The moiré potential in the $MoTe_2/WSe_2$ moiré superlattice with no twisting is formed due to the mismatch of the lattice constants of the two layers. There is another experiment on MIT in twisted WSe_2 [47]. The situation in twisted WSe_2 seems rather different from $MoTe_2/WSe_2$ moiré superlattice. Inside the "insulator phase," the resistivity $\rho(T)$ at some displacement fields first increases with decreasing temperature, and eventually the plot seems to saturate at a finite value, which is much lower than the resistivity observed in the $MoTe_2/WSe_2$ moiré superlattice near the MIT. Hence the MIT of twisted WSe_2 could be of a different nature: between the metallic phase and the insulator phase, there could be an intermediate phase with an order at nonzero momentum and reduced size of electron Fermi pockets.

Correlated insulators at other fractional fillings $\nu = p/q$ have been reported in various TMD moiré systems [48–51]. Although the nature of the MIT at these fillings has not been looked into carefully, here we briefly discuss the theory for the possible continuous MIT at general fractional filling $\nu = p/q$. As long as $q > 2$, even for parton construction I, the bosonic parton b will have fractional filling, and hence the insulator phase of b cannot be a trivial incompressible state without translation symmetry breaking or topological order. Here we would like to acknowledge that charge fractionalization for interacting electron system at fractional electron number per unit cell was discussed in previous literature [122], using similar formalism as the parton construction I. At electron filling $\nu = 1/q$, the boson filling $\nu_b = 2/q$; if we only consider nearest neighbor hopping of the vortex, the insulator has commensurate density wave that spontaneously breaks the translation symmetry, and the MIT is described by Eq. (4) with $N = q$ for odd integer q, $N = q/2$ for $q = 4k + 2$, and $N = q$ for $q = 4k$. The electron charge will further fractionalize at the continuous MIT. In parton construction I, there are in total N species of the charge carriers each carrying electric charge $e^* = e/N$. Hence the estimate of ρ_b is $\rho_b \sim Nh/e^2$.

For parton construction II, with electron filling $\nu = 1/q$, the boson filling for each spin-valley flavor is $\nu_b = 1/q$. Again, if only nearest neighbor hopping of the vortices is considered, the MIT is described by Eq. (4) with $N = q$ for odd integer q, $N = 2q$ for even integer q. The field theory describing the MIT is two copies of Eq. (4): ψ_j, A_μ, and a_μ should all carry a spin index α. There are in total $N_b = 2N$ species of the charge carriers each carrying electric charge $e^* = e/N$. Hence the estimate of ρ_b is $\rho_b \sim Nh/(2e^2)$. If we consider further neighbor hopping like in Sec. III, the charge carriers may carry even smaller fractional charge, and hence larger ρ_b.

Here, we would like to discuss some subtlety regarding the conductivity σ_b of the bosonic parton. In a generic theory with momentum conservation, one expects a finite overlap between the electric current and the conversed momentum. Such a finite overlap would lead to a Drude peak in the (optical) conductivity (see Ref. [120] for a review), $\sigma(\omega) = \sigma_Q + \mathcal{D}[(i/\omega) + \delta(\omega)]$, where $\mathcal{D} > 0$ is the Drude weight and ω is the frequency. In a theory with an exact particle-hole symmetry, this overlap between the electric current and momentum is strictly zero and, consequently, the Drude weight $\mathcal{D}$ vanishes. In the MIT considered in this paper and previous literature such as Refs. [54,55,70], the theories that govern the bosonic partons all have an emergent particle-hole symmetry. This emergent particle-hole symmetry is expected to produce a Drude weight that vanishes at zero temperature; namely, $\mathcal{D} \to 0$ as $T \to 0$. If there is a finite momentum relaxation time τ_p induced by, for example, disorder, the Drude peak should take the form $\mathcal{D}/\tau_p^{-1} - i\omega$ and should be viewed as an extra correction, when we take $\omega \to 0$, to the bosonic parton dc conductivity σ_b calculated for the MIT. Since $\mathcal{D}$ vanishes as $T \to 0$ due to the emergent particle-hole symmetry, the dc limit, i.e., $\omega \to 0$, of the Drude peak becomes a small correction to the bosonic parton dc conductivity σ_b at low temperature.

There is another subtlety associated with the bosonic parton conductivity due to extra hydrodynamical corrections and the purely two-dimensional nature of the system. It was known (see, for example, Ref. [123] for a review) that, when momentum is strictly conversed, even in the presence of particle-hole symmetry, hydrodynamical fluctuations lead to a logarithmic correction to the optical conductivity that scale as $\log(\tau_{\text{th}}\omega)$. Here, τ_{th} is the timescale of local thermalization [124] and can be estimated as $\sim T^{-1}$. This hydrodynamical correction to the conductivity diverges in the dc limit. This divergence is due to the long-lived hydrodynamical mode associated with the conserved momentum. As we mentioned before, in real systems disorder and umklapp process always induce a finite momentum relaxation time τ_p. The diverging hydrodynamical correction is only valid when $\tau_p \gg \tau_{\text{th}} \sim T^{-1}$, meaning momentum is strictly conserved over the thermalization timescale, where the hydrodynamical description becomes applicable. When the temperature T is low compared to τ_p^{-1}, hydrodynamical corrections are cut off by τ_p^{-1} and are again expected to be small corrections to the bosonic parton conductivity calculated in the rest of this paper. In fact, the divergent hydrodynamical correction may be already cut off at a higher temperature scale that is favorable to us, as the crossover

scale is suppressed by a large factor depending on the dimensionless entropy density of the system [124].

We would like to stress that the optical conductivity $\sigma(\infty)$ which is much easier to evaluate theoretically (see Sec. III for an example) is free of these subtleties, and we encourage future experiments to measure the optical conductivity at the MIT as well.

In recent years very impressive progress has been made on numerically simulating interacting fermionic systems (for examples, see Refs. [125–128]). It is conceivable that an extended Hubbard model with spin-orbit coupling can be constructed on the triangular lattice, and by changing the parameter (for example, the strength of the spin-orbit coupling), two types of interaction-driven MIT may be realized, one described by the original theory [54,56], the other described by our current theory. Predictions made in these two theories, such as different universality classes and transport properties at the MIT, different scalings of quasiparticle weight, and the existence of the spinon Fermi surface in the insulator phase, can potentially be directly tested through various numerical methods on the extended Hubbard model. We leave this to future exploration.

ACKNOWLEDGMENTS

The authors thank L. Balents, Luca Delacretaz, Sung-Sik Lee, C. Nayak, T. Senthil, and Kevin Slagle for very helpful discussions. C. X. is supported by NSF Grant No. DMR-1920434 and the Simons Investigator program; Z.-X. L. is supported by the Simons Collaborations on Ultra-Quantum Matter, Grant No. 651440 (LB); M. Y. was supported in part by the Gordon and Betty Moore Foundation through Grant No. GBMF8690 to UCSB, and by the NSF Grant No. PHY-1748958.

APPENDIX A: FIELD THEORIES FOR $N = 6$ and $N = 12$ OF SCENARIO (1)

In Appendix B, we derive the projective symmetry group transformation for the low-energy vortex modes of scenario (1). For $N = 6$, with symmetries $R_{2\pi/3}$, translation, $P_x\mathcal{T}$, and P_y, the PSG-invariant interactions between the vortex fields ψ_a beyond Eq. (4) take the following form:

$$\begin{aligned}\mathcal{L}^{(1)\prime}[\psi_a] = {} & u_1\sum_{a=0}^{2}(|\psi_{2a}|^2+|\psi_{2a+1}|^2)^2+u_2\left(\sum_{a=0}^{5}|\psi_a|^2\right)^2\\ & +v_1\left(\sum_{a=0}^{5}\psi_a^2\right)\left(\sum_{a=0}^{5}(\psi_a^*)^2\right)+v_2\sum_{a=0}^{2}(\psi_{2a}^2+\psi_{2a+1}^2)[(\psi_{2a}^*)^2+(\psi_{2a+1}^*)^2]\\ & +w_1\sum_{a=0}^{2}(|\psi_{2a}|^2-|\psi_{2a+1}|^2)(\psi_{2a+2}\psi_{2a+3}^*+\psi_{2a+2}^*\psi_{2a+3})+w_2\left\{\sum_{a=0}^{2}(\psi_{2a}^2-\psi_{2a+1}^2)\psi_{2a+2}^*\psi_{2a+3}^*+\text{c.c.}\right\}+\cdots.\end{aligned} \tag{A1}$$

Here the dots stand for terms higher than the quartic order. The parameters $\{u_1, u_2, v_1, v_2, w_1, w_2\}$ in Eq. (A1) are all real, and the index a for ψ_a is regarded as cyclic modulo 6.

In addition to the quartic terms, the gauge-invariant density wave order parameter can couple to the Fermi surface of the fermionic partons, and quartic terms of ψ_a with singularity in the frequency space can be generated as was pointed out by Ref. [86], such as $|\omega||S_{\omega,q}|^2$, where $S_{\omega,q}$ is a bilinear of ψ_a. This coupling only arises for scenario (1). For scenario (2) discussed in the main text, the 3D XY^* fixed point should be stable against symmetry allowed perturbations; the field theory Eq. (14) is also stable against coupling to the fermionic parton Fermi surface.

Although we do not aim to give a full discussion of the fate of the infrared limit of scenario (1), in the current work we establish the formalism for this problem that one can use in the future. As we explained in the previous paragraph, after integrating out the fermion that is connected by the finite momentum of the density wave order parameter, a term is generated $\sim|\omega||S_{\omega,q}|^2$, where $S = \psi^\dagger T\psi$ and T is an $N\times N$ matrix. One can introduce a new field Φ through the Hubbard-Stratonovich transformation, and ψ_a will interact with the Φ field [129]. We start with the first line of Eq. (A1). The field theory Eq. (4) with u_1 and u_2 in Eq. (A1) can be reformulated by introducing multiple Lagrange multipliers λ_i:

$$\begin{aligned}\mathcal{L}^{(1)} = {} & \sum_{a=0}^{N-1}|(\partial-iA)\psi_a|^2+i\sum_{i=1}^{N_1}\lambda_i\left(\sum_{\tau=1}^{N_2}|\psi_{\tau,i}|^2\right)\\ & +i\Phi\psi^\dagger T\psi;\\ \langle\lambda_i(\vec{q})\lambda_{i'}(-\vec{q})\rangle = {} & \frac{8}{N_2}|q|\delta_{i,i'},\\ \langle A_\mu(\vec{q})A_\nu(-\vec{q})\rangle = {} & \frac{16}{N}\left(\frac{\delta_{\mu\nu}-q_\mu q_\nu/q^2}{|q|}\right),\\ \langle\Phi(\vec{q})\Phi(-\vec{q})\rangle = {} & g|\omega|.\end{aligned} \tag{A2}$$

Here $N = N_1N_2$, and for the real system with $N = 6, N_1 = 3$ and $N_2 = 2$. Introducing λ_i for each index i physically means

that we are investigating the theory near the point with a $SU(N_2)$ symmetry for each index i, rather than the original CP^{N-1} theory with a large $SU(N)$ flavor symmetry. This is analogous to the "easy-plane bosonic QED_3" considered in Ref. [130]. The actions of λ_i and the transverse component of gauge field A are generated by integrating out the fields ψ_a. One possible way to proceed with the calculation is that we can fix N_1, and take $1/N_2$ as a small parameter. When g is the same order of $1/N_2$, the interaction between ψ_a and the Φ field will lead to the contribution comparable with that arising from coupling to λ_i and A. The calculation would be analogous to the one formulated in Ref. [89], where the nonlocal interaction on top of a bosonic QED flows to a new fixed point. One can evaluate the scaling behaviors (such as relevance or irrelevance in the IR) of the v and w terms in the second and third lines in Eq. (A1) at this new fixed point. By exploring the parameter space of g, $1/N_2$, and different choice of matrix T, it is possible to identify a finite region where Eq. (A2) corresponds to a stable fixed point where the v and w terms in Eq. (A1) are irrelevant.

The same strategy can be applied to the situation with $N = 12$. With long moiré lattice constants, the sixfold rotation $R_{\pi/3}$ also becomes a good approximate symmetry. Together with $R_{\pi/3}$, the quartic terms in the field theory for $N = 12$ (refer to the phase diagram in Fig. 2) are

$$\begin{aligned}\mathcal{L}^{(1)\prime}[\psi_{\sigma,\tau,i}] = {} & u_1\sum_{\sigma,i}\left(\sum_{\tau}|\psi_{\sigma,\tau,i}|^2\right)^2 + u_2\left(\sum_{\sigma\tau i}|\psi_{\sigma\tau i}|^2\right)^2 + v_1\sum_{\sigma,i\neq i'}\left(\sum_{\tau}|\psi_{\sigma,\tau,i}|^2\right)\left(\sum_{\tau'}|\psi_{\sigma,\tau',i'}|^2\right)\\ & + v_2\sum_{i}\left(\sum_{\tau}|\psi_{+,\tau,i}|^2\right)\left(\sum_{\tau'}|\psi_{-,\tau',i}|^2\right) + w_1\left|\sum_{i,\tau}\psi_{+,\tau,i}\psi_{-,\tau,i}\right|^2\\ & + iw_2\left(\sum_{i,\tau,\tau'}\psi^*_{+,\tau,i+1}\psi^*_{-,\tau,i+1}\psi_{+,\tau',i}\psi_{-,\tau',i} - \text{H.c.}\right).\end{aligned} \tag{A3}$$

Here the 12 modes are labeled by $\psi_{\sigma,\tau,i}$ in which $\tau = \pm$ labels two degenerate modes at the same momentum, $\sigma = \pm$ labels two sets of momenta that are each connected by $R_{2\pi/3}$, and $i = 0, 1, 2 \bmod 3$ labels these three momenta within each set.

We can again start with the first line of Eq. (A3), and introduce Lagrange multiplier $\lambda_{\sigma,i}$ which couples to the ψ_a fields as $\sum_{\tau=1}^{N_2}\lambda_{\sigma,i}|\psi_{\sigma,\tau,i}|^2$. Note that we have generalized τ to $1, \ldots, N_2$. Then the Hubbard-Stratonovich transformation can introduce new fields that couple to ψ_a to account for the singular terms generated through interacting with the Fermi surface. A combined perturbation theory of $1/N_2$ and g can again determine the relevance or irrelevance of the second and third lines of Eq. (A3). In particular, the two terms in the second line of Eq. (A3) are indeed irrelevant with large N_2, as the scaling dimension of $\sum_\tau|\psi_{\sigma,\tau,i}|^2$ is 2 with large N_2.

APPENDIX B: PSG TRANSFORMATION FOR $N = 6$ IN SCENARIO (1)

Under the boson-vortex duality, the dual vortex theory on the hexagonal lattice takes the form

$$H = \sum_{\langle ij\rangle} -t_{ij}\phi_i^*\phi_j + H'_\phi + V_\phi + \cdots, \quad t_{ij} = te^{-iA_{ij}}. \tag{B1}$$

Here H'_ϕ describes hopping terms between further neighbors. The potential V_ϕ includes a quadratic term $\sum_i r|\phi_i|^2$ which tunes through the phase transition.

When t_{ij} is nonzero only for nearest neighbor links on the dual honeycomb lattice, and it takes positive sign on the solid links and negative sign on the dashed links in Fig. 1 due to the π flux of A_μ through each hexagon, there are four minima of the vortex band structure in the Brillouin zone (Fig. 2). We label the four minimum modes from 0 to 3, each having momentum (k_x, k_y):

$$\mathbf{Q}_{0,1} = \mathbf{K} = \left(\frac{2\pi}{3\sqrt{3}}, 0\right), \qquad \mathbf{Q}_{2,3} = \mathbf{K}' = \left(\frac{\pi}{3\sqrt{3}}, \frac{\pi}{3}\right). \tag{B2}$$

With further neighbor vortex hopping (refer to the phase diagram in Fig. 2), the minima of the vortex band structure can shift to the M points, similar to Ref. [80]. When the degenerate minima are shifted to the M points (Fig. 2), the six corresponding momenta are

$$\mathbf{Q}_{0,1} = \left(\frac{\pi}{2\sqrt{3}}, -\frac{\pi}{6}\right), \quad \mathbf{Q}_{2,3} = \left(\frac{\pi}{2\sqrt{3}}, \frac{\pi}{6}\right), \quad \mathbf{Q}_{4,5} = \left(0, \frac{\pi}{3}\right). \tag{B3}$$

Similar to the four minima case, the vortex field can be expanded using these six modes as

$$\phi_{n,\mathbf{r}} \sim \sum_{a=0}^{5}\psi_a v_{a,n}e^{i\mathbf{Q}_a\cdot\mathbf{r}}. \tag{B4}$$

The coefficients $v_{a,n}$ are solved from the band structure.

The symmetries of the theory for one single valley must include translation T_1, T_2, threefold rotation $R_{2\pi/3}$, $P_x\mathcal{T}$ (as illustrated in Fig. 3). These transformations do not mix the two valleys. In the following we derive the PSG matrices of these symmetries. We first need the form of the transformations when acting on the 8 sites in each unit cell:

$$T_{1,2}(\phi_{n,\mathbf{k}}) = \sum_m (t_{1,2})_{nm}\phi_{m,\mathbf{k}}, \qquad t_1 = \begin{pmatrix} 0 & 0 & 0 & 0 & 0 & 0 & 1 & 0 \\ 0 & 0 & 0 & 0 & 0 & 0 & 0 & 1 \\ 0 & 0 & 0 & -1 & 0 & 0 & 0 & 0 \\ 0 & 0 & 1 & 0 & 0 & 0 & 0 & 0 \\ 0 & 0 & 0 & 0 & 0 & 1 & 0 & 0 \\ 0 & 0 & 0 & 0 & -1 & 0 & 0 & 0 \\ -1 & 0 & 0 & 0 & 0 & 0 & 0 & 0 \\ 0 & -1 & 0 & 0 & 0 & 0 & 0 & 0 \end{pmatrix}, \qquad t_2 = \begin{pmatrix} 0 & 0 & 1 & 0 & 0 & 0 & 0 & 0 \\ 0 & 0 & 0 & 0 & 1 & 0 & 0 & 0 \\ -1 & 0 & 0 & 0 & 0 & 0 & 0 & 0 \\ 0 & 0 & 0 & 0 & 0 & 0 & -1 & 0 \\ 0 & -1 & 0 & 0 & 0 & 0 & 0 & 0 \\ 0 & 0 & 0 & 0 & 0 & 0 & 0 & 1 \\ 0 & 0 & 0 & 1 & 0 & 0 & 0 & 0 \\ 0 & 0 & 0 & 0 & 0 & -1 & 0 & 0 \end{pmatrix}, \tag{B5}$$

$$R_{2\pi/3}(\phi_{n,\mathbf{k}}) = (r_{\pi/3})_{nm}\phi_{m,R_{2\pi/3}\mathbf{k}}, \qquad r_{2\pi/3} = \begin{pmatrix} 1 & 0 & 0 & 0 & 0 & 0 & 0 & 0 \\ 0 & 0 & 0 & 0 & 1 & 0 & 0 & 0 \\ 0 & 0 & 0 & 0 & 0 & 0 & 1 & 0 \\ 0 & 0 & 1 & 0 & 0 & 0 & 0 & 0 \\ 0 & 0 & 0 & 0 & 0 & 1 & 0 & 0 \\ 0 & 1 & 0 & 0 & 0 & 0 & 0 & 0 \\ 0 & 0 & 0 & 1 & 0 & 0 & 0 & 0 \\ 0 & 0 & 0 & 0 & 0 & 0 & 0 & 1 \end{pmatrix}, \tag{B6}$$

$$P_x\mathcal{T}(\phi_{n,\mathbf{k}}) = (p_x t)_{nm}\phi_{m,-P_x\mathbf{k}}, \qquad (p_x t)_{ab} = \begin{pmatrix} 1 & 0 & 0 & 0 & 0 & 0 & 0 & 0 \\ 0 & 1 & 0 & 0 & 0 & 0 & 0 & 0 \\ 0 & 0 & 0 & -1 & 0 & 0 & 0 & 0 \\ 0 & 0 & -1 & 0 & 0 & 0 & 0 & 0 \\ 0 & 0 & 0 & 0 & 0 & 1 & 0 & 0 \\ 0 & 0 & 0 & 0 & 1 & 0 & 0 & 0 \\ 0 & 0 & 0 & 0 & 0 & 0 & -1 & 0 \\ 0 & 0 & 0 & 0 & 0 & 0 & 0 & -1 \end{pmatrix}. \tag{B7}$$

Besides these symmetries, here we argue that, if the system does have an effective Hubbard model description with two local Wannier orbitals per unit cell (one for each valley), P_y is also a good symmetry of the Hubbard model, as long as the valley mixing is negligible, which is a justified assumption with long wavelength moiré potential modulation. Let us first assume there is no valley mixing, then for each valley the band structure of the moiré miniband is described by a tight binding model with one orbital per site on the moiré triangular lattice. The hopping amplitude $t(\theta)$ along angle θ must satisfy the following relations based on the explicit $P_x\mathcal{T}$ and translation symmetry:

$$t(\theta) = t^*(\pi - \theta), \qquad t^*(\theta) = t(\pi + \theta). \tag{B8}$$

We can easily show that $t(\theta) = t(-\theta)$; namely, the system should have a P_y symmetry.

However, when there is valley mixing, t becomes a 2×2 matrix with off-diagonal terms that mix two valleys. A 2×2 hopping matrix t should satisfy four symmetries, P_x, $\mathcal{T}$, translation, and $R_{2\pi/3}$ rotation. A natural choice of P_x and $\mathcal{T}$ on t is

$$P_x\colon\ t(\theta) \to \sigma^x t(\pi - \theta)\sigma^x, \qquad \mathcal{T}\colon\ t(\theta) \to (i\sigma^y)t^*(-i\sigma^y), \tag{B9}$$

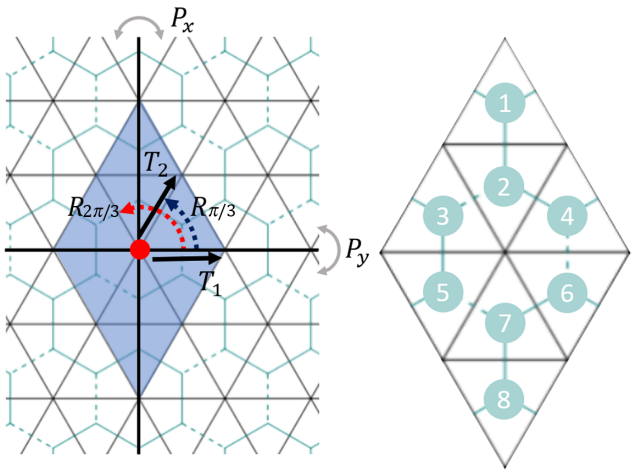

FIG. 3. Crystal symmetry of the triangular lattice, the nearest neighbor hopping amplitudes of the vortices, and the unit cell after taking into account of the sign of t_{ij}.

and the translation symmetry plus Hermicity demands $t^\dagger(\theta) = t(\pi+\theta)$. P_y does not change the valley indices; if P_y takes $t(\theta)$ to $t(-\theta)$, there exists a valley mixing term $t(\theta) \sim i\sigma^x \sin(3\theta)$ that preserves all the symmetries mentioned above, but breaks P_y; while if P_y takes $t(\theta)$ to $\sigma^z t(-\theta)\sigma^z$, this term becomes $t(\theta) \sim i\sigma^y \cos(3\theta)$.

P_y acts on the ϕ bosons as

$$P_y(\phi_{n,\mathbf{k}}) = (p_y)_{nm}\phi^*_{m,-P_y\mathbf{k}},$$

$$(p_y)_{ab} = \begin{pmatrix} 0&0&0&0&0&0&0&1\\ 0&0&0&0&0&0&1&0\\ 0&0&0&0&1&0&0&0\\ 0&0&0&0&0&1&0&0\\ 0&0&1&0&0&0&0&0\\ 0&0&0&1&0&0&0&0\\ 0&1&0&0&0&0&0&0\\ 1&0&0&0&0&0&0&0 \end{pmatrix}. \quad \text{(B10)}$$

Furthermore, in the case with long moiré lattice constant, we additionally have the sixfold rotation $R_{\pi/3}$:

$$R_{\pi/3}(\phi_{n,\mathbf{k}}) = (r_{\pi/3})_{nm}\phi_{m,R_{\pi/3}\mathbf{k}},$$

$$(r_{\pi/3})_{ab} = \begin{pmatrix} 0&0&0&0&0&0&0&-1\\ 0&0&-1&0&0&0&0&0\\ 0&0&0&0&1&0&0&0\\ 0&1&0&0&0&0&0&0\\ 0&0&0&0&0&0&-1&0\\ 0&0&0&-1&0&0&0&0\\ 0&0&0&0&0&1&0&0\\ 1&0&0&0&0&0&0&0 \end{pmatrix}. \quad \text{(B11)}$$

In the position space, the transformation rules can be summarized as

$$G(\phi_{n,\mathbf{r}}) = \sum_{m=1}^{8} g_{n,m}\phi_{m,\mathbf{r}'_m}, \quad \text{(B12)}$$

in which $\mathbf{r}'_m$ is the center of the unit cell of field ϕ_m which is obtained by certain site in the original unit cell (centered at $\mathbf{r}$) after transformation under symmetry operation G. For example, under T_1, $\mathbf{r}'_7 = \mathbf{r}'_8 = \mathbf{r} + 2\mathbf{a}_2$, because sites 1 and 2 at unit cell $\mathbf{r}$ are transformed into sites 7 and 8 in the nearby enlarged unit cell which is centered at $\mathbf{r} + 2\mathbf{a}_2$. In general, we can write the transformation as $\mathbf{r}'_m = G\mathbf{r} + \vec{\Delta}_{G,m}$, in which $\vec{\Delta}_{G,m}$ is a constant that does not depend on $\mathbf{r}$, and $G\mathbf{r}$ is the coordinate of the center of the unit cell after spacial symmetry G.

Now we plug in the low-energy expansions of $\phi_{n_\mathbf{k}}$ around the minima into the equation, which yields

$$\sum_{a=0}^{N-1} G(\psi_a) v_{a,n} e^{i\mathbf{Q}_a\cdot\mathbf{r}} = \sum_{a=0}^{N-1}\sum_{m=1}^{8} \psi_a g_{nm} v_{m,a} e^{i\mathbf{Q}_a\cdot\mathbf{r}'_m}. \quad \text{(B13)}$$

The relation can be viewed as a vector identity with n being the vector index on both sides. Because all the vectors $v_{a,n}(a = 0, \ldots, N-1)$ are orthogonal to each other, we can multiply the conjugated vector $v^*_{b,n}$ on both sides and sum over n:

$$G(\psi_b) e^{i\mathbf{Q}_b\cdot\mathbf{r}} = \sum_{a=0}^{N-1}\sum_{m,n=1}^{8} \psi_a v^*_{b,n} g_{n,m} v_{a,m} e^{i\mathbf{Q}_a\cdot\mathbf{r}'_m}. \quad \text{(B14)}$$

For this equation to hold for all $\mathbf{r}$, the rhs needs to have the same momentum. This requires $\mathbf{Q}_b = G^{-1}\mathbf{Q}_a$, which can only be satisfied by two possible choices of a (recall that in the convention of eight-site unit cell, each momentum $\mathbf{Q}_a$ always has twofold degeneracy for all N), denoted by a_1 and a_2. Thus we eventually have

$$G(\psi_b) = \sum_{m,n=1}^{8} v^\dagger_{b,n} g_{nm} v_{a_1,m} e^{i\mathbf{Q}_{a_1}\cdot\vec{\Delta}_{G,m}} \times \psi_{a_1} + \sum_{m,n=1}^{8} v^\dagger_{b,n} g_{nm} v_{a_2,m} e^{i\mathbf{Q}_{a_2}\cdot\vec{\Delta}_{G,m}} \times \psi_{a_2}. \quad \text{(B15)}$$

The final results can be organized into $N \times N$ matrices. For $N = 6$, the transformations read

$$T_{1,2}(\psi_a) = (\mathfrak{t}_{1,2})_{ab}\psi_b,$$

$$(\mathfrak{t}_1)_{ab} = \begin{pmatrix} -1 & 0 & 0 & 0 & 0 & 0 \\ 0 & 1 & 0 & 0 & 0 & 0 \\ 0 & 0 & 0 & 1 & 0 & 0 \\ 0 & 0 & 1 & 0 & 0 & 0 \\ 0 & 0 & 0 & 0 & 0 & 1 \\ 0 & 0 & 0 & 0 & -1 & 0 \end{pmatrix},$$

$$(\mathfrak{t}_2)_{ab} = \begin{pmatrix} 0 & 1 & 0 & 0 & 0 & 0 \\ -1 & 0 & 0 & 0 & 0 & 0 \\ 0 & 0 & 1 & 0 & 0 & 0 \\ 0 & 0 & 0 & -1 & 0 & 0 \\ 0 & 0 & 0 & 0 & 0 & -1 \\ 0 & 0 & 0 & 0 & -1 & 0 \end{pmatrix}, \tag{B16}$$

$$R_{2\pi/3}(\psi_a) = (\mathfrak{R}_{2\pi/3})_{ab}\psi_b,$$

$$(\mathfrak{R}_{2\pi/3})_{ab} = \begin{pmatrix} 0 & 0 & 0 & 0 & 1 & 0 \\ 0 & 0 & 0 & 0 & 0 & 1 \\ -1 & 0 & 0 & 0 & 0 & 0 \\ 0 & -1 & 0 & 0 & 0 & 0 \\ 0 & 0 & 1 & 0 & 0 & 0 \\ 0 & 0 & 0 & 1 & 0 & 0 \end{pmatrix}, \tag{B17}$$

$$P_x\mathcal{T}(\psi_a) = (\mathfrak{P}_x\mathfrak{T})_{ab}\psi_b,$$

$$(\mathfrak{P}_x\mathfrak{T})_{ab} = \frac{1}{\sqrt{2}}\begin{pmatrix} 0 & 0 & 1 & -1 & 0 & 0 \\ 0 & 0 & -1 & -1 & 0 & 0 \\ 1 & -1 & 0 & 0 & 0 & 0 \\ -1 & -1 & 0 & 0 & 0 & 0 \\ 0 & 0 & 0 & 0 & 1 & -1 \\ 0 & 0 & 0 & 0 & -1 & -1 \end{pmatrix}, \tag{B18}$$

$$P_y(\psi_a) = (\mathfrak{P}_y)_{ab}\psi_b^*,$$

$$(\mathfrak{P}_y)_{ab} = \frac{1}{\sqrt{2}}\begin{pmatrix} 0 & 0 & 1 & 1 & 0 & 0 \\ 0 & 0 & 1 & -1 & 0 & 0 \\ 1 & 1 & 0 & 0 & 0 & 0 \\ 1 & -1 & 0 & 0 & 0 & 0 \\ 0 & 0 & 0 & 0 & 1 & 1 \\ 0 & 0 & 0 & 0 & 1 & -1 \end{pmatrix}, \tag{B19}$$

$$R_{\pi/3}(\psi_a) = (\mathfrak{R}_{\pi/3})_{ab}\psi_b,$$

$$(\mathfrak{R}_{\pi/3})_{ab} = \begin{pmatrix} 0 & 0 & 0 & -1 & 0 & 0 \\ 0 & 0 & 1 & 0 & 0 & 0 \\ 0 & 0 & 0 & 0 & 0 & 1 \\ 0 & 0 & 0 & 0 & -1 & 0 \\ 0 & 1 & 0 & 0 & 0 & 0 \\ -1 & 0 & 0 & 0 & 0 & 0 \end{pmatrix}. \tag{B20}$$

Deep inside the vortex condensate phase with $r \ll 0$ in Eq. (4), the vector $\vec{\Psi} = (\psi_0, \psi_1, \psi_2, \psi_3, \psi_4, \psi_5)$ can have different condensates depending on the parameters in Eq. (A1). Without loss of generality we set $\sum_{a=0}^{5} |\psi_a|^2 = 1$. The two figures in Fig. 4 illustrate the density waves of the bosonic parton centered at the bonds and the sites on the moiré triangular lattice that correspond to two different possible condensates of $\vec{\Psi}$. The density on the bond l is inferred from $t_{ij}\langle\phi_i^*\phi_j\rangle$, with ij being the link on the dual honeycomb lattice that is dual to l, and t_{ij} takes the sign according to the gauge convention of Fig. 1. The operator $t_{ij}\langle\phi_i^*\phi_j\rangle$ is the energy density in terms of vortex fields, and the modulation of this operator should correspond to the valence bond solid of the original bosonic parton. We also consider an operator centered on site p of the original lattice (plaquette of the dual lattice): $\sum_{\langle ij\rangle\in p} t_{ij}\langle\phi_i^*\phi_j\rangle$, with the summation over the links that surround the plaquette p on the dual honeycomb lattice, whose center hosts the site p of the original moiré triangular lattice. In both cases, $\langle\phi_i^*\phi_j\rangle$ is evaluated using Eq. (B4) and the value of $\vec{\Psi}$ which minimizes the quartic energy. The left-hand pattern in Fig. 4 is a rather common valence bond solid configuration for either spin-1/2 system or hard core boson on the triangular lattice. If one started with the construction I of the parton construction, the discussion in this appendix corresponds to the original electron system with an average 1/2 electron per unit cell (the filling considered in Ref. [49]); while for construction II, the discussion here applies to one electron per unit cell,

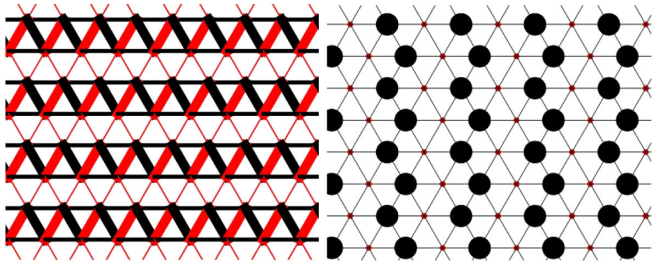

FIG. 4. Some possible density wave patterns of the original boson that correspond to different condensate of ψ_a with $a = 0, \ldots, 5$. The left- and right-hand patterns correspond to $\vec{\Psi} \sim (1, 0, 0, 0, 0, 0)$ and $\vec{\Psi} \sim (0, 1/\sqrt{2}, 1/2, -1/2, 0, 0)$, respectively.

and the analysis in this appendix corresponds to one of the two spin or valley flavors of the system.

APPENDIX C: DUAL OF THE VORTEX THEORY

Here we derive the Lagrangian written in terms of the fractionally charged bosonic partons for scenario (1). We start with Eq. (4) in the main text:

$$\mathcal{L}^{(1)} = \sum_{j=0}^{N-1} |(\partial_\mu - iA_\mu)\psi_j|^2 + r|\psi_j|^2 + \frac{i}{2\pi} A \wedge d(a + eA_{\text{ext}}) + \cdots. \tag{C1}$$

To facilitate the calculation of the dc resistivity which we discuss in the next appendix, we need to "dual back" to the charge carriers, which requires deforming Eq. (C1) with an easy-plane anisotropy $\sum_j |\psi_j|^4$. The bosonic fractional charge carriers φ_j are the vortices of the vortex fields ψ_j. We first take the standard duality for ψ_j, and Eq. (C1) becomes

$$\mathcal{L}^{(1)} = \sum_{j=0}^{N-1} |(\partial - i\tilde{A}_j)\varphi_j|^2 + \tilde{r}|\varphi_j|^2 + \frac{i}{2\pi}\tilde{A}_j \wedge dA + \frac{i}{2\pi} A \wedge d(a + eA_{\text{ext}}) + \cdots. \tag{C2}$$

According to the basic duality relation, the current of ψ_j, i.e., J_{ψ_j}, is mapped to $d\tilde{A}_j$. Now integrating out A would lead to the following constraint for the rest of the gauge fields:

$$\sum_j \tilde{A}_j - a - eA_{\text{ext}} = 0. \tag{C3}$$

From this constraint we can take $\tilde{A}_j$ as

$$\tilde{A}_j = \tilde{a}_j + \frac{1}{N} a + \frac{e}{N} A_{\text{ext}}, \qquad \sum_j \tilde{a}_j = 0. \tag{C4}$$

Hence the dual of the dual theory becomes

$$\mathcal{L}^{(1)} = \sum_{j=0}^{N-1} \left| \left(\partial - i\tilde{a}_j - i\frac{1}{N} a - i\frac{e}{N} A_{\text{ext}} \right) \varphi_j \right|^2 + \tilde{r}|\varphi_j|^2 + \cdots. \tag{C5}$$

The gauge fields $\tilde{a}_j$ are still subject to the constraint $\sum_j \tilde{a}_j = 0$. φ_j carries e/N charge of external electromagnetic gauge field; it also carries charge $1/N$ of gauge field a which is shared with the fermionic parton f_α.

For scenario (2) the theory in terms of fractional parton φ is much simpler: there is only one flavor of φ for each valley, and there is no extra continuous gauge fields $\tilde{a}$ besides gauge field a. Following the calculation in Ref. [70], one can generalize this one flavor of φ in each valley to an $\mathbf{N}$ component of bosons:

$$\mathcal{L}^{(2)} = \sum_{l=1}^{\mathbf{N}} \left| \left(\partial - i\frac{1}{N} a - i\frac{e}{N} A_{\text{ext}} \right) \varphi^l \right|^2 + i\lambda|\varphi^l|^2 + \cdots, \tag{C6}$$

and the bosons will scatter with both gauge field a and field λ which is introduced as a Lagrange multiplier. The fact that φ^l carries charge $1/N$ of gauge field a does not change the scattering rate through the large-$\mathbf{N}$ calculation, as the gauge charge cancels out in the calculation of scattering rate through the large-$\mathbf{N}$ approach. Compared with scenario (2), in scenario (1) the parton φ_j is also coupled to extra gauge fields $\tilde{a}_j$, which will lead to extra scattering to the charge carriers.

When computing the resistivity, especially the dc resistivity of scenario (1), we also rely on a large-$\mathbf{N}$ generalization; namely, we need to introduce an extra $l = 1, \ldots, \mathbf{N}$ index for each component of fractional charge field: φ_j^l.

APPENDIX D: dc RESISTIVITY JUMP IN SCENARIO (1)

In this appendix, we present a detailed computation of the dc resistivity jump in scenario (1) of MIT, i.e., the scenario when the insulator has a density wave. We start with Eq. (C5). The resistivity jump at the MIT is given by the universal resistivity of the bosonic sector of the system ρ_b at the MIT. First, one can prove a generalized Ioffe-Larkin rule, which combines the resistivity of each parton φ_j into ρ_b:

$$\rho_b = \frac{\hbar}{e^2} \left(\sum_{j=0}^{N-1} \rho_{b,j} \right), \tag{D1}$$

where $\rho_{b,j}$ is the resistivity of each parton φ_j, when the charge of φ_j is taken to be 1. This generalized Ioffe-Larkin rule can be proven by formally integrating out φ_j, gauge fields $\tilde{a}_j$ and a from Eq. (C5), and eventually arriving at a response function of A_{ext}. At each level of the path integral, we keep a quadratic form of the action, i.e., the random phase approximation. This Ioffe-Larkin rule is independent of the assignment of electric charges on each parton.

To compute ρ_b, we formulate the quantum Boltzmann equation for the φ_j fields of a given valley. The computation follows that for ρ_b at the MIT without charge fractionalization [70], where the gauge-field dynamics needs to be modified due to the charge fractionalization, which we explain in detail below for comparison. Note that ρ_b can be finite without momentum relaxation due to the emergent particle-hole symmetry. Furthermore, the two-in two-out scatterings among the φ_j fields are enough to relax the current and generate finite dc resistivity. For simplicity, we consider the scattering between the φ_j and emergent gauge fields in Eq. (C5), where the gauge fields are in thermal equilibrium and their dynamics is acquired due to

the coupling with the matter fields φ_j and f. Here, we argue that treating the gauge fields as in thermal equilibrium is a legitimate approximation. First, the gauge field a couples to the spinon field f, which is sensitive to impurities and relaxes momentum fast. Second, diagrammatically, the two-in two-out scatterings between the φ_j fields that give finite dc resistivity can be captured by the φ_j scattering with the emergent gauge fields.

To simplify the computation of the gauge field dynamics, it is convenient to express Eq. (C5) in terms of the gauge field $\tilde{A}_j$ [Eq. (C3)], together with the effective action for the spinon field, the dual theory reads

$$\mathcal{L}^{(1)} = \sum_{j=0}^{N-1} |(\partial - i\tilde{A}_j)\varphi_j|^2 + \tilde{r}|\varphi_j|^2 + \bar{f}\left[\partial_\tau - \mu - i\sum_{j=0}^{N-1}\tilde{A}_{j,0} + ieA_{\mathrm{ext},0} + \frac{1}{2m}\left(\nabla - i\sum_{j=0}^{N-1}\tilde{\boldsymbol{A}}_j + ie\boldsymbol{A}_{\mathrm{ext}}\right)^2\right] f + \cdots. \quad \text{(D2)}$$

Integrating out φ_j and f fields, the gauge-field propagators read

$$D_{ij}^{(\tilde{A})} = -i\langle \mathrm{T}_t \tilde{A}_i \tilde{A}_j\rangle = \begin{cases} \frac{\Pi_b^J + (N-1)\Pi_f^J}{(\Pi_b^J)^2 + N\Pi_b^J\Pi_f^J} & \text{if } i = j \\ \frac{-\Pi_f^J}{(\Pi_b^J)^2 + N\Pi_b^J\Pi_f} & \text{if } i \neq j, \end{cases} \quad \text{(D3)}$$

where Π_b^J, Π_f^J is the current-current correlation function for φ_j and f fields, respectively.

For a controlled systematic calculation of transport, we introduce a large number of (complex) rotor and spinon flavors $\mathbf{N}$ with the constraint $\sum_{l=1}^{\mathbf{N}} |\varphi_j^l|^2 = 1$ for all $j = 0, 1, \ldots, N-1$, and only the $l = 1$ component couples to A_{ext}. The $\mathbf{N} = 1$ limit will be taken at the end. The effective action for the extended model becomes

$$\begin{aligned}\mathcal{L} = &\sum_{j=0}^{N-1}\left[\sum_{l=1}^{\mathbf{N}} |(\partial - i\tilde{A}_j)\varphi_j^l|^2 + i\lambda_j\left(\sum_{l=1}^{\mathbf{N}}|\varphi_j^l|^2 - 1\right) + \frac{1}{2g^2}(\epsilon_{\mu\nu\lambda}\partial_\nu \tilde{A}_{j,\lambda})^2\right] \\ &+ \sum_{l=1}^{\mathbf{N}} \bar{f}_l\left[\partial_\tau - \mu - i\sum_{j=0}^{N-1}\tilde{A}_{j,0} + ieA_{\mathrm{ext},0}\delta_{l,1} + \frac{1}{2m}\left(\nabla - i\sum_{j=0}^{N-1}\tilde{\boldsymbol{A}}_j + ie\boldsymbol{A}_{\mathrm{ext}}\delta_{l,1}\right)^2\right] f_l + \cdots. \end{aligned} \quad \text{(D4)}$$

Using the Fourier expansion for the electrically charged rotor $\varphi_j^{l=1}$ in terms of the holons (+) and doublons (-),

$$\varphi_j^{l=1} = \int_{\boldsymbol{k}} \alpha_{+,j}(t,\boldsymbol{k})e^{i\boldsymbol{k}\cdot\boldsymbol{x}} + \alpha_{-,j}(t,\boldsymbol{k})e^{-i\boldsymbol{k}\cdot\boldsymbol{x}}, \quad \text{(D5)}$$

the conductivity $\sigma_{b,j} = \rho_{b,j}^{-1}$ can be obtained as

$$\sigma_{b,j} = \langle J_{x,j}\rangle/E_x, \quad \langle J_{x,j}\rangle = \int_{\boldsymbol{k}}\sum_{s=\pm} s\frac{\boldsymbol{k}}{\epsilon_{\boldsymbol{k}}} f_{s,j}(t,\boldsymbol{k}), \quad \text{(D6)}$$

where we define the distribution for holon ($s = +$) and doublon ($s = -$) as $f_{s,j} = \langle \alpha_{s,j}^\dagger(t,\boldsymbol{k})\alpha_{s,j}(t,\boldsymbol{k})\rangle$, and they satisfy the quantum Boltzmann equation as

$$(\partial_t + s\boldsymbol{E}\cdot\partial_{\boldsymbol{k}})f_{s,j}(t,\boldsymbol{k}) = \frac{1}{2\mathbf{N}}(I_{\lambda_j}[f_{\pm,j}] + I_{\tilde{A}_j}[f_{\pm,j}]). \quad \text{(D7)}$$

Note that the gauge choice in Eq. (D2) ensures that $f_{s,j}$ are decoupled and equal for different j within the approximation that $\tilde{A}_j$ is in thermal equilibrium, so the subindex j will be dropped unless there is ambiguity. The rhs of Eq. (D7) reads

$$\begin{aligned}\mathrm{rhs} = &\frac{1}{2\mathbf{N}}\int_0^\infty \frac{d\Omega}{\pi}\int\frac{d^2\boldsymbol{q}}{(2\pi)^2}\{\tau_\lambda \mathrm{Im}D^{(\lambda)}(\Omega,\boldsymbol{q}) + \tau_{\tilde{A}}\mathrm{Im}D_{ii}^{(\tilde{A})}(\Omega,\boldsymbol{q})\} \\ &\times\left(\frac{2\pi\delta(\epsilon_{\boldsymbol{k}} - \epsilon_{\boldsymbol{k}+\boldsymbol{q}} + \Omega)}{4\epsilon_{\boldsymbol{k}}\epsilon_{\boldsymbol{k}+\boldsymbol{q}}}\{f_s(t,\boldsymbol{k})[1 + f_s(t,\boldsymbol{k}+\boldsymbol{q})]n_{\boldsymbol{q}}(\Omega) - [1 + f_s(t,\boldsymbol{k})]f_s(t,\boldsymbol{k}+\boldsymbol{q})[1 + n_{\boldsymbol{q}}(\Omega)]\}\right. \\ &+\frac{2\pi\delta(\epsilon_{\boldsymbol{k}} - \epsilon_{\boldsymbol{k}+\boldsymbol{q}} - \Omega)}{4\epsilon_{\boldsymbol{k}}\epsilon_{\boldsymbol{k}+\boldsymbol{q}}}\{f_s(t,\boldsymbol{k})[1 + f_s(t,\boldsymbol{k}+\boldsymbol{q})][1 + n_{\boldsymbol{q}}(\Omega)] - [1 + f_s(t,\boldsymbol{k})]f_s(t,\boldsymbol{k}+\boldsymbol{q})n_{\boldsymbol{q}}(\Omega)\} \\ &\left.+\frac{2\pi\delta(-\epsilon_{\boldsymbol{k}} - \epsilon_{\boldsymbol{k}+\boldsymbol{q}} + \Omega)}{4\epsilon_{\boldsymbol{k}}\epsilon_{\boldsymbol{k}+\boldsymbol{q}}}\{f_s(t,\boldsymbol{k})f_s(t,\boldsymbol{k}+\boldsymbol{q})[1 + n_{\boldsymbol{q}}(\Omega)] - [1 + f_s(t,\boldsymbol{k})][1 + f_s(t,\boldsymbol{k}+\boldsymbol{q})]n_{\boldsymbol{q}}(\Omega)\}\right), \end{aligned} \quad \text{(D8)}$$

TABLE II. Rotor conductivity ($\sigma_{b,j}$) and resistivity jump ρ_b at the MIT with fractionally charged bosonic parton $e_* = e/N$.

N	1	2	3	4	5	6	…	∞
$\sigma_{b,j}(e^2/\hbar)$	0.021	0.029	0.034	0.036	0.038	0.039		0.047
$\rho_b(h/e^2)$	3.72	5.41	7.09	8.76	10.44	12.11		$[3.62 + 1.68(N-1)]$

where $\tau_\lambda = -1$ and $\tau_{\tilde{A}} = (2\boldsymbol{k} \times \hat{\boldsymbol{q}})^2$ come from the bare vertex functions.

$\mathrm{Im}D^{(\lambda)}, \mathrm{Im}D^{(\tilde{A})}$ physically denote the density of states of the emergent fields that scatter with φ, which are broad in the $(\Omega, \boldsymbol{q})$ space due to the couplings with the φ fields. Below, we ignore the bare dynamics. $D^{(\lambda),(\tilde{A})}$ in the large-$\mathbf{N}$ limit reads

$$\begin{aligned} D^{(\lambda)}(\Omega, \boldsymbol{q}) &= \frac{1}{\Pi_b}, \\ D^{(\tilde{A})}_{ii}(\Omega, \boldsymbol{q}) &= \frac{\Pi_b^J + (N-1)\Pi_f^J}{(\Pi_b^J)^2 + N\Pi_b^J\Pi_f^J} \\ &= \frac{N-1}{N}\frac{1}{\Pi_b^J} + \frac{1}{N}\frac{1}{\Pi_b^J + N\Pi_f^J}, \end{aligned} \tag{D9}$$

where $D^{(\tilde{A})}_{ii}$ reduces to the MIT without charge fractionalization as discussed in Ref. [70] when $N = 1$. For $N > 1$, as only the linear combination of $\tilde{A}_j$, i.e., $\sum_{j=0}^{N-1}\tilde{A}_j$ couples to the spinon field f and is Landau damped, there is a factor $1/N$ for the Landau damped component of the gauge-field propagator $D^{(\tilde{A})}_{ii}$, which may also be understood as the a component of gauge field in Eq. (C5). The rest does not receive Landau damping, and is determined solely by Π_b^J. Note that as $\mathrm{Im}\Pi_f^J \gg \mathrm{Im}\Pi_b^J$ in the limit $\mu \gg T$, the Landau damped component can be approximated as $(1/N)[1/(\Pi_b^J + N\Pi_f^J)] \approx (1/N)\{1/[(\Pi_b^J(\Omega = 0, \boldsymbol{q}) + N\Pi_f^J(\Omega, \boldsymbol{q})]\}$, and can be treated in the same way as Ref. [70] for the gauge field a. On the other hand, the first term in $D^{(\tilde{A})}_{ii}$ should be determined for generic Ω, $\boldsymbol{q}$. Using the standard expression for polarizations Π,

$$\begin{aligned} \Pi_b(\Omega, \boldsymbol{q}) &= \frac{T}{2}\sum_m \int_{\boldsymbol{k}} \tau_\lambda \frac{1}{(\nu_m + \Omega_n)^2 + \epsilon^2_{\boldsymbol{k}+\boldsymbol{q}}}\frac{1}{\nu_m^2 + \epsilon^2_{\boldsymbol{k}}}\Big|_{i\Omega_n \to \Omega + i\delta}, \\ \Pi_b^J(\Omega, \boldsymbol{q}) &= \frac{T}{2}\sum_m \int_{\boldsymbol{k}} \tau_{\tilde{A}} \frac{1}{(\nu_m + \Omega_n)^2 + \epsilon^2_{\boldsymbol{k}+\boldsymbol{q}}}\frac{1}{\nu_m^2 + \epsilon^2_{\boldsymbol{k}}}\Big|_{i\Omega_n \to \Omega + i\delta}, \\ \Pi_f^J(\Omega, \boldsymbol{q}) &= -\frac{T}{2}\sum_m \int_{\boldsymbol{k}} \frac{(2\boldsymbol{k} \times \hat{\boldsymbol{q}})^2}{(2m)^2}\frac{1}{i(\omega_m + \Omega_n) - \xi_{\boldsymbol{k}+\boldsymbol{q}}}\frac{1}{i\omega_m - \xi_{\boldsymbol{k}}}\Big|_{i\Omega_n \to \Omega + i\delta}. \end{aligned} \tag{D10}$$

Equation (D7) can be solved self-consistently. In Table II, we show $\sigma_{b,j}$ and the final resistivity $\rho_b = (N\sigma_{b,j}^{-1})/2$ at different N; again the factor of $1/2$ arises from the two spin and valley flavors. ρ_b increases roughly linearly with N, and the fit of the data points at different N gives

$$\rho_b = [R^{(0)} + R^{(1)}(N-1)]\frac{h}{e^2} = [3.62 + 1.68(N-1)]\frac{h}{e^2}. \tag{D11}$$

[1] Yuan Cao, Valla Fatemi, Ahmet Demir, Shiang Fang, Spencer L. Tomarken, Jason Y. Luo, Javier D. Sanchez-Yamagishi, Kenji Watanabe, Takashi Taniguchi, Efthimios Kaxiras *et al.*, *Correlated Insulator Behaviour at Half-Filling in Magic-Angle Graphene Superlattices*, Nature (London) **556**, 80 (2018).

[2] Yuan Cao, Valla Fatemi, Shiang Fang, Kenji Watanabe, Takashi Taniguchi, Efthimios Kaxiras, and Pablo Jarillo-Herrero, *Unconventional Superconductivity in Magic-Angle Graphene Superlattices*, Nature (London) **556**, 43 (2018).

[3] Guorui Chen, Lili Jiang, Shuang Wu, Bosai Lyu, Hongyuan Li, Bheema Lingam Chittari, Kenji Watanabe, Takashi Taniguchi, Zhiwen Shi, Jeil Jung *et al.*, *Evidence of a Gate-Tunable Mott Insulator in a Trilayer Graphene moiré Superlattice*, Nat. Phys. **15**, 237 (2019).

[4] Matthew Yankowitz, Shaowen Chen, Hryhoriy Polshyn, Yuxuan Zhang, K. Watanabe, T. Taniguchi, David Graf, Andrea F. Young, and Cory R. Dean, *Tuning Superconductivity in Twisted Bilayer Graphene*, Science **363**, 1059 (2019).

[5] Yu Saito, Jingyuan Ge, Kenji Watanabe, Takashi Taniguchi, and Andrea F. Young, *Independent Superconductors and Correlated Insulators in Twisted Bilayer Graphene*, Nat. Phys. **16**, 926 (2020).

[6] Petr Stepanov, Ipsita Das, Xiaobo Lu, Ali Fahimniya, Kenji Watanabe, Takashi Taniguchi, Frank H. L. Koppens, Johannes Lischner, Leonid Levitov, and Dmitri K. Efetov,

Untying the Insulating and Superconducting Orders in Magic-Angle Graphene, Nature (London) **583**, 375 (2020).

[7] Guorui Chen, Aaron L. Sharpe, Patrick Gallagher, Ilan T. Rosen, Eli J. Fox, Lili Jiang, Bosai Lyu, Hongyuan Li, Kenji Watanabe, Takashi Taniguchi *et al.*, *Signatures of Tunable Superconductivity in a Trilayer Graphene moiré Superlattice*, Nature (London) **572**, 215 (2019).

[8] Xiaomeng Liu, Zeyu Hao, Eslam Khalaf, Jong Yeon Lee, Yuval Ronen, Hyobin Yoo, Danial Haei Najafabadi, Kenji Watanabe, Takashi Taniguchi, Ashvin Vishwanath *et al.*, *Tunable Spin-Polarized Correlated States in Twisted Double Bilayer Graphene*, Nature (London) **583**, 221 (2020).

[9] Yuan Cao, Daniel Rodan-Legrain, Oriol Rubies-Bigorda, Jeong Min Park, Kenji Watanabe, Takashi Taniguchi, and Pablo Jarillo-Herrero, *Tunable Correlated States and Spin-Polarized Phases in Twisted Bilayer-Bilayer Graphene*, Nature (London) **583**, 215 (2020).

[10] Yuan Cao, Debanjan Chowdhury, Daniel Rodan-Legrain, Oriol Rubies-Bigorda, Kenji Watanabe, Takashi Taniguchi, T. Senthil, and Pablo Jarillo-Herrero, *Strange Metal in Magic-Angle Graphene with near Planckian Dissipation*, Phys. Rev. Lett. **124**, 076801 (2020).

[11] Hryhoriy Polshyn, Matthew Yankowitz, Shaowen Chen, Yuxuan Zhang, K. Watanabe, T. Taniguchi, Cory R. Dean, and Andrea F. Young, *Large Linear-in-Temperature Resistivity in Twisted Bilayer Graphene*, Nat. Phys. **15**, 1011 (2019).

[12] Rafi Bistritzer and Allan H. MacDonald, *Moiré Bands in Twisted Double-Layer Graphene*, Proc. Natl. Acad. Sci. U.S.A. **108**, 12233 (2011).

[13] J. M. B. Lopes dos Santos, N. M. R. Peres, and A. H. Castro Neto, *Continuum Model of the Twisted Graphene Bilayer*, Phys. Rev. B **86**, 155449 (2012).

[14] Cenke Xu and Leon Balents, *Topological Superconductivity in Twisted Multilayer Graphene*, Phys. Rev. Lett. **121**, 087001 (2018).

[15] Noah F. Q. Yuan and Liang Fu, *Model for the Metal-Insulator Transition in Graphene Superlattices and Beyond*, Phys. Rev. B **98**, 045103 (2018).

[16] Hiroki Isobe, Noah F. Q. Yuan, and Liang Fu, *Unconventional Superconductivity and Density Waves in Twisted Bilayer Graphene*, Phys. Rev. X **8**, 041041 (2018).

[17] Mikito Koshino, Noah F. Q. Yuan, Takashi Koretsune, Masayuki Ochi, Kazuhiko Kuroki, and Liang Fu, *Maximally Localized Wannier Orbitals and the Extended Hubbard Model for Twisted Bilayer Graphene*, Phys. Rev. X **8**, 031087 (2018).

[18] Alex Thomson, Shubhayu Chatterjee, Subir Sachdev, and Mathias S. Scheurer, *Triangular Antiferromagnetism on the Honeycomb Lattice of Twisted Bilayer Graphene*, Phys. Rev. B **98**, 075109 (2018).

[19] J. F. Dodaro, S. A. Kivelson, Y. Schattner, X. Q. Sun, and C. Wang, *Phases of a Phenomenological Model of Twisted Bilayer Graphene*, Phys. Rev. B **98**, 075154 (2018).

[20] Hoi Chun Po, Liujun Zou, Ashvin Vishwanath, and T. Senthil, *Origin of Mott Insulating Behavior and Superconductivity in Twisted Bilayer Graphene*, Phys. Rev. X **8**, 031089 (2018).

[21] Jian Kang and Oskar Vafek, *Symmetry, Maximally Localized Wannier States, and a Low-Energy Model for Twisted Bilayer Graphene Narrow Bands*, Phys. Rev. X **8**, 031088 (2018).

[22] Liujun Zou, Hoi Chun Po, Ashvin Vishwanath, and T. Senthil, *Band Structure of Twisted Bilayer Graphene: Emergent Symmetries, Commensurate Approximants, and Wannier Obstructions*, Phys. Rev. B **98**, 085435 (2018).

[23] Yi-Zhuang You and Ashvin Vishwanath, *Superconductivity from Valley Fluctuations and Approximate SO(4) Symmetry in a Weak Coupling Theory of Twisted Bilayer Graphene*, npj Quantum Mater. **4**, 16 (2019).

[24] Nick Bultinck, Eslam Khalaf, Shang Liu, Shubhayu Chatterjee, Ashvin Vishwanath, and Michael P. Zaletel, *Ground State and Hidden Symmetry of Magic-Angle Graphene at Even Integer Filling*, Phys. Rev. X **10**, 031034 (2020).

[25] Nick Bultinck, Shubhayu Chatterjee, and Michael P. Zaletel, *Mechanism for Anomalous Hall Ferromagnetism in Twisted Bilayer Graphene*, Phys. Rev. Lett. **124**, 166601 (2020).

[26] Fengcheng Wu, A. H. MacDonald, and Ivar Martin, *Theory of Phonon-Mediated Superconductivity in Twisted Bilayer Graphene*, Phys. Rev. Lett. **121**, 257001 (2018).

[27] B. Lian, Z. Wang, and B. A. Bernevig, *Twisted Bilayer Graphene: A Phonon-Driven Superconductor*, Phys. Rev. Lett. **122**, 257002 (2019).

[28] Jong Yeon Lee, Eslam Khalaf, Shang Liu, Xiaomeng Liu, Zeyu Hao, Philip Kim, and Ashvin Vishwanath, *Theory of Correlated Insulating Behaviour and Spin-Triplet Superconductivity in Twisted Double Bilayer Graphene*, Nat. Commun. **10**, 5333 (2019).

[29] Eslam Khalaf, Shubhayu Chatterjee, Nick Bultinck, Michael P. Zaletel, and Ashvin Vishwanath, *Charged Skyrmions and Topological Origin of Superconductivity in Magic-Angle Graphene*, Sci. Adv. **7**, eabf5299 (2021).

[30] Yichen Xu, Xiao-Chuan Wu, Chao-Ming Jian, and Cenke Xu, *Orbital Order and Possible Non-Fermi Liquid in Moiré Systems*, Phys. Rev. B **101**, 205426 (2020).

[31] Rafael M. Fernandes and Jörn W. F. Venderbos, *Nematicity with a Twist: Rotational Symmetry Breaking in a moiré Superlattice*, Sci. Adv. **6**, eaba8834 (2020).

[32] Bheema Lingam Chittari, Guorui Chen, Yuanbo Zhang, Feng Wang, and Jeil Jung, *Gate-Tunable Topological Flat Bands in Trilayer Graphene Boron-Nitride Moiré Superlattices*, Phys. Rev. Lett. **122**, 016401 (2019).

[33] M. Serlin, C. L. Tschirhart, H. Polshyn, Y. Zhang, J. Zhu, K. Watanabe, T. Taniguchi, L. Balents, and A. F. Young, *Intrinsic Quantized Anomalous Hall Effect in a moiré Heterostructure*, Science **367**, 900 (2020).

[34] Ya-Hui Zhang, Dan Mao, Yuan Cao, Pablo Jarillo-Herrero, and T. Senthil, *Nearly Flat Chern Bands in Moiré Superlattices*, Phys. Rev. B **99**, 075127 (2019).

[35] Guorui Chen, Aaron L. Sharpe, Eli J. Fox, Ya-Hui Zhang, Shaoxin Wang, Lili Jiang, Bosai Lyu, Hongyuan Li, Kenji Watanabe, Takashi Taniguchi *et al.*, *Tunable Correlated Chern Insulator and Ferromagnetism in a moiré Superlattice*, Nature (London) **579**, 56 (2020).

[36] Cécile Repellin and T. Senthil, *Chern Bands of Twisted Bilayer Graphene: Fractional Chern Insulators and Spin Phase Transition*, arXiv:1912.11469.

[37] P. Stepanov, M. Xie, T. Taniguchi, K. Watanabe, X. Lu, A. H. MacDonald, B. A. Bernevig, and D. K. Efetov, *Competing Zero-Field Chern Insulators in Superconducting Twisted Bilayer Graphene*, Phys. Rev. Lett. **127**, 197701 (2021).

[38] Shaowen Chen, Minhao He, Ya-Hui Zhang, Valerie Hsieh, Zaiyao Fei, K. Watanabe, T. Taniguchi, David H. Cobden, Xiaodong Xu, Cory R. Dean *et al.*, *Electrically Tunable Correlated and Topological States in Twisted Monolayer-Bilayer Graphene*, Nat. Phys. **17**, 374 (2021).

[39] Andrew T. Pierce, Yonglong Xie, Jeong Min Park, Eslam Khalaf, Seung Hwan Lee, Yuan Cao, Daniel E. Parker, Patrick R. Forrester, Shaowen Chen, Kenji Watanabe, Takashi Taniguchi, Ashvin Vishwanath, Pablo Jarillo-Herrero, and Amir Yacoby, *Unconventional Sequence of Correlated Chern Insulators in Magic-Angle Twisted Bilayer Graphene*, Nat. Phys. **17**, 1210 (2021).

[40] Xiao-Chuan Wu, Yichen Xu, Chao-Ming Jian, and Cenke Xu, *Interacting Valley Chern Insulator and Its Topological Imprint on Moiré Superconductors*, Phys. Rev. B **100**, 155138 (2019).

[41] Fengcheng Wu, Timothy Lovorn, Emanuel Tutuc, and A. H. MacDonald, *Hubbard Model Physics in Transition Metal Dichalcogenide Moiré Bands*, Phys. Rev. Lett. **121**, 026402 (2018).

[42] Haining Pan, Fengcheng Wu, and Sankar Das Sarma, *Band Topology, Hubbard Model, Heisenberg Model, and Dzyaloshinskii-Moriya Interaction in Twisted Bilayer* WSe_2, Phys. Rev. Research **2**, 033087 (2020).

[43] Yanhao Tang, Lizhong Li, Tingxin Li, Yang Xu, Song Liu, Katayun Barmak, Kenji Watanabe, Takashi Taniguchi, Allan H. MacDonald, Jie Shan, and Kin Fai Mak, WSe_2/WS_2 *Moiré Superlattices: A New Hubbard Model Simulator*, arXiv:1910.08673.

[44] Aaron Szasz, Johannes Motruk, Michael P. Zaletel, and Joel E. Moore, *Chiral Spin Liquid Phase of the Triangular Lattice Hubbard Model: A Density Matrix Renormalization Group Study*, Phys. Rev. X **10**, 021042 (2020).

[45] Aaron Szasz and Johannes Motruk, *Phase Diagram of the Anisotropic Triangular Lattice Hubbard Model*, Phys. Rev. B **103**, 235132 (2021).

[46] Tingxin Li, Shengwei Jiang, Lizhong Li, Yang Zhang, Kaifei Kang, Jiacheng Zhu, Kenji Watanabe, Takashi Taniguchi, Debanjan Chowdhury, Liang Fu *et al.*, *Continuous Mott Transition in Semiconductor moiré Superlattices*, Nature (London) **597**, 350 (2021).

[47] Augusto Ghiotto, En-Min Shih, Giancarlo S. S. G. Pereira, Daniel A. Rhodes, Bumho Kim, Jiawei Zang, Andrew J. Millis, Kenji Watanabe, Takashi Taniguchi, James C. Hone *et al.*, *Quantum Criticality in Twisted Transition Metal Dichalcogenides*, Nature (London) **597**, 345 (2021).

[48] Emma C. Regan, Danqing Wang, Chenhao Jin, M. Iqbal Bakti Utama, Beini Gao, Xin Wei, Sihan Zhao, Wenyu Zhao, Zuocheng Zhang, Kentaro Yumigeta *et al.*, *Mott and Generalized Wigner Crystal States in* WSe_2/WS_2 *moiré Superlattices*, Nature (London) **579**, 359 (2020).

[49] Chenhao Jin, Zui Tao, Tingxin Li, Yang Xu, Yanhao Tang, Jiacheng Zhu, Song Liu, Kenji Watanabe, Takashi Taniguchi, James C. Hone *et al.*, *Stripe Phases in* WSe_2/WS_2 *moiré Superlattices*, Nat. Mater. **20**, 940 (2021).

[50] Yang Xu, Song Liu, Daniel A. Rhodes, Kenji Watanabe, Takashi Taniguchi, James Hone, Veit Elser, Kin Fai Mak, and Jie Shan, *Correlated Insulating States at Fractional Fillings of moiré Superlattices*, Nature (London) **587**, 214 (2020).

[51] Xiong Huang, Tianmeng Wang, Shengnan Miao, Chong Wang, Zhipeng Li, Zhen Lian, Takashi Taniguchi, Kenji Watanabe, Satoshi Okamoto, Di Xiao *et al.*, *Correlated Insulating States at Fractional Fillings of the* WS_2/WSe_2 *moiré Lattice*, Nat. Phys. **17**, 715 (2021).

[52] Elliott Lieb, Theodore Schultz, and Daniel Mattis, *Two Soluble Models of an Antiferromagnetic Chain*, Ann. Phys. (N.Y.) **16**, 407 (1961).

[53] M. B. Hastings, *Lieb-Schultz-Mattis in Higher Dimensions*, Phys. Rev. B **69**, 104431 (2004).

[54] Sung-Sik Lee and Patrick A. Lee, *U(1) Gauge Theory of the Hubbard Model: Spin Liquid States and Possible Application to* κ-$BEDTTTF_2Cu_2CN_3$, Phys. Rev. Lett. **95**, 036403 (2005).

[55] T. Senthil, *Critical Fermi Surfaces and Non-Fermi Liquid Metals*, Phys. Rev. B **78**, 035103 (2008).

[56] T. Senthil, *Theory of a Continuous Mott Transition in Two Dimensions*, Phys. Rev. B **78**, 045109 (2008).

[57] David F. Mross and T. Senthil, *Charge Friedel Oscillations in a Mott Insulator*, Phys. Rev. B **84**, 041102(R) (2011).

[58] Min-Chul Cha, Matthew P. A. Fisher, S. M. Girvin, Mats Wallin, and A. Peter Young, *Universal Conductivity of Two-Dimensional Films at the Superconductor-Insulator Transition*, Phys. Rev. B **44**, 6883 (1991).

[59] B. Spivak, S. V. Kravchenko, S. A. Kivelson, and X. P. A. Gao, *Colloquium: Transport in Strongly Correlated Two Dimensional Electron Fluids*, Rev. Mod. Phys. **82**, 1743 (2010).

[60] L. B. Ioffe and A. I. Larkin, *Gapless Fermions and Gauge Fields in Dielectrics*, Phys. Rev. B **39**, 8988 (1989).

[61] Matthew P. A. Fisher, G. Grinstein, and S. M. Girvin, *Presence of Quantum Diffusion in Two Dimensions: Universal Resistance at the Superconductor-Insulator Transition*, Phys. Rev. Lett. **64**, 587 (1990).

[62] Rosario Fazio and Dario Zappalà, *ϵ Expansion of the Conductivity at the Superconductor-Mott-Insulator Transition*, Phys. Rev. B **53**, R8883 (1996).

[63] Jurij Šmakov and Erik Sørensen, *Universal Scaling of the Conductivity at the Superfluid-Insulator Phase Transition*, Phys. Rev. Lett. **95**, 180603 (2005).

[64] William Witczak-Krempa, Erik S. Sørensen, and Subir Sachdev, *The Dynamics of Quantum Criticality Revealed by Quantum Monte Carlo and Holography*, Nat. Phys. **10**, 361 (2014).

[65] Kun Chen, Longxiang Liu, Youjin Deng, Lode Pollet, and Nikolay Prokof'ev, *Universal Conductivity in a Two-Dimensional Superfluid-to-Insulator Quantum Critical System*, Phys. Rev. Lett. **112**, 030402 (2014).

[66] Shai M. Chester, Walter Landry, Junyu Liu, David Poland, David Simmons-Duffin, Ning Su, and Alessandro Vichi,

Carving out OPE Space and Precise O(2) Model Critical Exponents, J. High Energy Phys. 06 (2020) 142.

[67] D. B. Haviland, Y. Liu, and A. M. Goldman, *Onset of Superconductivity in the Two-Dimensional Limit*, Phys. Rev. Lett. **62**, 2180 (1989).

[68] Y. Liu, K. A. McGreer, B. Nease, D. B. Haviland, G. Martinez, J. W. Halley, and A. M. Goldman, *Scaling of the Insulator-to-Superconductor Transition in Ultrathin Amorphous Bi Films*, Phys. Rev. Lett. **67**, 2068 (1991).

[69] S. J. Lee and J. B. Ketterson, *Critical Sheet Resistance for the Suppression of Superconductivity in Thin Mo-C Films*, Phys. Rev. Lett. **64**, 3078 (1990).

[70] William Witczak-Krempa, Pouyan Ghaemi, T. Senthil, and Yong Baek Kim, *Universal Transport near a Quantum Critical Mott Transition in Two Dimensions*, Phys. Rev. B **86**, 245102 (2012).

[71] V. J. Emery and S. A. Kivelson, *Superconductivity in Bad Metals*, Phys. Rev. Lett. **74**, 3253 (1995).

[72] N. E. Hussey, K. Takenaka, and H. Takagi, *Universality of the Mott-Ioffe-Regel Limit in Metals*, Philos. Mag. **84**, 2847 (2004).

[73] Michael E Peskin, *Mandelstam-'t Hooft Duality in Abelian Lattice Models*, Ann. Phys. (N.Y.) **113**, 122 (1978).

[74] C. Dasgupta and B. I. Halperin, *Phase Transition in a Lattice Model of Superconductivity*, Phys. Rev. Lett. **47**, 1556 (1981).

[75] Matthew P. A. Fisher and D. H. Lee, *Correspondence between Two-Dimensional Bosons and a Bulk Superconductor in a Magnetic Field*, Phys. Rev. B **39**, 2756 (1989).

[76] Leon Balents, Lorenz Bartosch, Anton Burkov, Subir Sachdev, and Krishnendu Sengupta, *Competing Orders and Non-Landau-Ginzburg-Wilson Criticality in (Bose) Mott Transitions*, Prog. Theor. Phys. Suppl. **160**, 314 (2005).

[77] A. A. Burkov and Leon Balents, *Superfluid-Insulator Transitions on the Triangular Lattice*, Phys. Rev. B **72**, 134502 (2005).

[78] R. Moessner and S. L. Sondhi, *Ising Models of Quantum Frustration*, Phys. Rev. B **63**, 224401 (2001).

[79] Cenke Xu and Subir Sachdev, *Global Phase Diagrams of Frustrated Quantum Antiferromagnets in Two Dimensions: Doubled Chern-Simons Theory*, Phys. Rev. B **79**, 064405 (2009).

[80] Kevin Slagle and Cenke Xu, *Quantum Phase Transition between the Z_2 Spin Liquid and Valence Bond Crystals on a Triangular Lattice*, Phys. Rev. B **89**, 104418 (2014).

[81] Cenke Xu and Leon Balents, *Quantum Phase Transitions around the Staggered Valence-Bond Solid*, Phys. Rev. B **84**, 014402 (2011).

[82] Cong-Jun Wu, Ian Mondragon-Shem, and Xiang-Fa Zhou, *Unconventional Bose-Einstein Condensations from Spin-Orbit Coupling*, Chin. Phys. Lett. **28**, 097102 (2011).

[83] Chunji Wang, Chao Gao, Chao-Ming Jian, and Hui Zhai, *Spin-Orbit Coupled Spinor Bose-Einstein Condensates*, Phys. Rev. Lett. **105**, 160403 (2010).

[84] Xiao-Tian Zhang and Gang Chen, *Infinity Scatter Infinity: Infinite Critical Boson Non-Fermi Liquid*, arXiv:2102.09272.

[85] Ethan Lake, T. Senthil, and Ashvin Vishwanath, *Bose-Luttinger Liquids*, Phys. Rev. B **104**, 014517 (2021).

[86] Seth Musser, T. Senthil, and Debanjan Chowdhury, *Theory of a Continuous Bandwidth-Tuned Wigner-Mott Transition*, arXiv:2111.09894.

[87] Tarun Grover and Ashvin Vishwanath, *Quantum Criticality in Topological Insulators and Superconductors: Emergence of Strongly Coupled Majoranas and Supersymmetry*, arXiv:1206.1332.

[88] Yichen Xu, Xiao-Chuan Wu, Chao-Ming Jian, and Cenke Xu, *Topological Edge and Interface States at Bulk Disorder-to-Order Quantum Critical Points*, Phys. Rev. B **101**, 184419 (2020).

[89] Chao-Ming Jian, Yichen Xu, Xiao-Chuan Wu, and Cenke Xu, *Continuous Néel-VBS Quantum Phase Transition in Non-Local One-Dimensional Systems with SO(3) Symmetry*, SciPost Phys. **10**, 33 (2021).

[90] Joseph Polchinski, *Low-Energy Dynamics of the Spinon-Gauge System*, Nucl. Phys. **B422**, 617 (1994).

[91] Chetan Nayak and Frank Wilczek, *Non-Fermi Liquid Fixed Point in $2+1$ Dimensions*, Nucl. Phys. **B417**, 359 (1994).

[92] Chetan Nayak and Frank Wilczek, *Renormalization Group Approach to Low Temperature Properties of a Non-Fermi Liquid Metal*, Nucl. Phys. **B430**, 534 (1994).

[93] Sung-Sik Lee, *Low-Energy Effective Theory of Fermi Surface Coupled with U(1) Gauge Field in $2+1$ Dimensions*, Phys. Rev. B **80**, 165102 (2009).

[94] David F. Mross, John McGreevy, Hong Liu, and T. Senthil, *Controlled Expansion for Certain Non-Fermi-Liquid Metals*, Phys. Rev. B **82**, 045121 (2010).

[95] Max A. Metlitski and Subir Sachdev, *Quantum Phase Transitions of Metals in Two Spatial Dimensions. I. Ising-Nematic Order*, Phys. Rev. B **82**, 075127 (2010).

[96] Max A. Metlitski and Subir Sachdev, *Quantum Phase Transitions of Metals in Two Spatial Dimensions. II. Spin Density Wave Order*, Phys. Rev. B **82**, 075128 (2010).

[97] Max A. Metlitski, David F. Mross, Subir Sachdev, and T. Senthil, *Cooper Pairing in Non-Fermi Liquids*, Phys. Rev. B **91**, 115111 (2015).

[98] Yuxuan Wang and Andrey V. Chubukov, *Enhancement of Superconductivity at the Onset of Charge-Density-Wave Order in a Metal*, Phys. Rev. B **92**, 125108 (2015).

[99] Ipsita Mandal, *Superconducting Instability in Non-Fermi Liquids*, Phys. Rev. B **94**, 115138 (2016).

[100] S. Lederer, Y. Schattner, E. Berg, and S. A. Kivelson, *Enhancement of Superconductivity near a Nematic Quantum Critical Point*, Phys. Rev. Lett. **114**, 097001 (2015).

[101] Yuxuan Wang, Artem Abanov, Boris L. Altshuler, Emil A. Yuzbashyan, and Andrey V. Chubukov, *Superconductivity near a Quantum-Critical Point: The Special Role of the First Matsubara Frequency*, Phys. Rev. Lett. **117**, 157001 (2016).

[102] Samuel Lederer, Yoni Schattner, Erez Berg, and Steven A. Kivelson, *Superconductivity and Non-Fermi Liquid Behavior near a Nematic Quantum Critical Point*, Proc. Natl. Acad. Sci. U.S.A. **114**, 4905 (2017).

[103] Liujun Zou and Debanjan Chowdhury, *Deconfined Metallic Quantum Criticality: A $U(2)$ Gauge-Theoretic Approach*, Phys. Rev. Research **2**, 023344 (2020).

[104] Ipsita Mandal, *Critical Fermi Surfaces in Generic Dimensions Arising from Transverse Gauge Field Interactions*, Phys. Rev. Research **2**, 043277 (2020).
[105] Pasquale Calabrese, Andrea Pelissetto, and Ettore Vicari, *The Critical Behavior of Magnetic Systems Described by Landau-Ginzburg-Wilson Field Theories*, arXiv:cond-mat/0306273.
[106] Sergei V. Isakov, Arun Paramekanti, and Yong Baek Kim, *Exotic Phase Diagram of a Cluster Charging Model of Bosons on the Kagome Lattice*, Phys. Rev. B **76**, 224431 (2007).
[107] T. Senthil, Ashvin Vishwanath, Leon Balents, Subir Sachdev, and Matthew P. A. Fisher, *Deconfined Quantum Critical Points*, Science **303**, 1490 (2004).
[108] T. Senthil, Leon Balents, Subir Sachdev, Ashvin Vishwanath, and Matthew P. A. Fisher, *Quantum Criticality beyond the Landau-Ginzburg-Wilson Paradigm*, Phys. Rev. B **70**, 144407 (2004).
[109] Yan-Cheng Wang, Meng Cheng, William Witczak-Krempa, and Zi Yang Meng, *Fractionalized Conductivity and Emergent Self-Duality near Topological Phase Transitions*, Nat. Commun. **12**, 5347 (2021).
[110] V. Kalmeyer and R. B. Laughlin, *Equivalence of the Resonating-Valence-Bond and Fractional Quantum Hall States*, Phys. Rev. Lett. **59**, 2095 (1987).
[111] Vadim Kalmeyer and R. B. Laughlin, *Theory of the Spin Liquid State of the Heisenberg Antiferromagnet*, Phys. Rev. B **39**, 11879 (1989).
[112] Meng Cheng, Michael Zaletel, Maissam Barkeshli, Ashvin Vishwanath, and Parsa Bonderson, *Translational Symmetry and Microscopic Constraints on Symmetry-Enriched Topological Phases: A View from the Surface*, Phys. Rev. X **6**, 041068 (2016).
[113] Michael Levin and Ady Stern, *Fractional Topological Insulators*, Phys. Rev. Lett. **103**, 196803 (2009).
[114] Maissam Barkeshli and John McGreevy, *Continuous Transition between Fractional Quantum Hall and Superfluid States*, Phys. Rev. B **89**, 235116 (2014).
[115] S. V. Isakov, R. G. Melko, and M. B. Hastings, *Universal Signatures of Fractionalized Quantum Critical Points*, Science **335**, 193 (2012).
[116] Silviu S. Pufu and Subir Sachdev, *Monopoles in* $2+1$*-Dimensional Conformal Field Theories with Global U(1) Symmetry*, J. High Energy Phys. 09 (2013) 127.
[117] Ethan Dyer, Márk Mezei, Silviu S. Pufu, and Subir Sachdev, *Scaling Dimensions of Monopole Operators in the CPNb!1 Theory in* $2+1$ *Dimensions*, J. High Energy Phys. 06 (2015) 037.
[118] Markus König, Steffen Wiedmann, Christoph Brüne, Andreas Roth, Hartmut Buhmann, Laurens W. Molenkamp, Xiao-Liang Qi, and Shou-Cheng Zhang, *Quantum Spin Hall Insulator State in HgTe Quantum Wells*, Science **318**, 766 (2007).
[119] Patrick A. Lee and Naoto Nagaosa, *Gauge Theory of the Normal State of High-*T_c *Superconductors*, Phys. Rev. B **46**, 5621 (1992).
[120] Sean A. Hartnoll, Andrew Lucas, and Subir Sachdev, *Holographic Quantum Matter* (The MIT Press, Cambridge, MA, 2018).
[121] Cody P. Nave and Patrick A. Lee, *Transport Properties of a Spinon Fermi Surface Coupled to a U(1) Gauge Field*, Phys. Rev. B **76**, 235124 (2007).
[122] Gang Chen, Hae-Young Kee, and Yong Baek Kim, *Fractionalized Charge Excitations in a Spin Liquid on Partially Filled Pyrochlore Lattices*, Phys. Rev. Lett. **113**, 197202 (2014).
[123] Pavel Kovtun, *Lectures on Hydrodynamic Fluctuations in Relativistic Theories*, J. Phys. A **45**, 473001 (2012).
[124] Luca V. Delacretaz, *Heavy Operators and Hydrodynamic Tails*, SciPost Phys. **9**, 34 (2020).
[125] Yoni Schattner, Samuel Lederer, Steven A. Kivelson, and Erez Berg, *Ising Nematic Quantum Critical Point in a Metal: A Monte Carlo Study*, Phys. Rev. X **6**, 031028 (2016).
[126] Xiao Yan Xu, Kai Sun, Yoni Schattner, Erez Berg, and Zi Yang Meng, *Non-Fermi Liquid at* $(2+1)$*D Ferromagnetic Quantum Critical Point*, Phys. Rev. X **7**, 031058 (2017).
[127] Hong-Chen Jiang and Thomas P. Devereaux, *Superconductivity in the Doped Hubbard Model and Its Interplay with Next-Nearest Hopping* t', Science **365**, 1424 (2019).
[128] Aaron Szasz, Johannes Motruk, Michael P. Zaletel, and Joel E. Moore, *Chiral Spin Liquid Phase of the Triangular Lattice Hubbard Model: A Density Matrix Renormalization Group Study*, Phys. Rev. X **10**, 021042 (2020).
[129] Ribhu K. Kaul and Subir Sachdev, *Quantum Criticality of U(1) Gauge Theories with Fermionic and Bosonic Matter in Two Spatial Dimensions*, Phys. Rev. B **77**, 155105 (2008).
[130] Sergio Benvenuti and Hrachya Khachatryan, *Easy-Plane* QED_3 *in the Large* N_f *Limit*, J. High Energy Phys. 05 (2019) 214.